medRxiv preprint doi: https://doi.org/10.1101/2021.06.07.21258504; this version posted June 11, 2021. The copyright holder for this preprint (which was not certified by peer review) is the author/funder, who has granted medRxiv a license to display the preprint in perpetuity. All rights reserved. No reuse allowed without permission.

Adaptive vaccination may be needed to extirpate COVID-19: Results from a runtime-alterable strain-drift and waning-immunity model

Wayne M. Getz[1,2,3], Richard Salter[3,4], Ludovica Luisa Vissat[1], James S. Koopman[5], Carl P. Simon[6]

[1]Dept. ESPM, UC Berkeley, CA 94720-3114, USA

[2]School of Mathematical Sciences, University of KwaZulu-Natal, South Africa

[3]Numerus, 850 Iron Point Rd., Folsom, CA 95630, USA

[4]Computer Science Dept., Oberlin College, Oberlin, Ohio, OH 44074, USA

[5]School of Public Health, University of Michigan, Ann Arbor, MI 48109, USA

[6]Gerald R. Ford School of Public Policy, University of Michigan, Ann Arbor, MI 48109, USA

Corresponding Author: Wayne M. Getz, wgetz@berkeley.edu

Author Contributions: JSK and CPS initiated the project, provided feedback on early drafts and participated in discussions. WMG designed and formulated the SEIVD-IBM model, drafted the manuscript, ran simulations, and produced the figures. RS designed and built the J-RAMP platform and wrote the code and informational text. LLV checked all the mathematical equations and code. Both RS and LLV contributed to the structure of the manuscript. All authors contributed to editing and adding text as needed.

Competing Interest Statements: none

Classification. Major: Biological Sciences; Minor: Biophysics and Computational Biology

Keywords: SARS-CoV-2, SEIR models, multivalent vaccines, escape mutations, strain/variant proliferation

NOTE: This preprint reports new research that has not been certified by peer review and should not be used to guide clinical practice.

medRxiv preprint doi: https://doi.org/10.1101/2021.06.07.21258504; this version posted June 11, 2021. The copyright holder for this preprint (which was not certified by peer review) is the author/funder, who has granted medRxiv a license to display the preprint in perpetuity. All rights reserved. No reuse allowed without permission.

Abstract

We developed an elaborated susceptible-infected-recovered (SIR) individual-based model (IBM) with pathogen strain drift, waning and cross immunity, implemented as a novel Java Runtime-Alterable-Model Platform (J-RAMP). This platform allows parameter values, process formulations, and scriptable runtime drivers to be easily added at the start of simulation. It includes facility for integration into the R statistical and other data analysis platforms. We selected a set of parameter values and process descriptions relevant to the current COVID-19 pandemic. These include pathogen-specific shedding, environmental persistence, host transmission and mortality, within-host pathogen mutation and replication, adaptive social distancing, and time dependent vaccine rate and strain valency specifications. Our simulations illustrate that if waning immunity outpaces vaccination rates, then vaccination rollouts may fail to contain the most transmissible strains. Our study highlights the need for adaptive vaccination rollouts, which depend on reliable real-time monitoring and surveillance of strain proliferation and reinfection data needed to ensure that vaccines target emerging strains and constrain escape mutations. Together with such data, our platform has the potential to inform the design of vaccination programs that extirpate rather than exacerbate local outbreaks. Finally, our RAMP concept promotes the development of highly flexible models that can be easily shared among researchers and policymakers not only addressing healthcare crises, but other types of environmental crises as well.

Significance Statement: Effective COVID-19 vaccine development has been unprecedented, but vaccinations are being delivered at contrasting rates across the globe. Here, using an innovative epidemiological Java runtime alterable modeling platform (J-RAMP), we demonstrate that seemingly reasonable vaccination programs may exacerbate rather than mitigate regional outbreaks when immune waning outpaces vaccinations and reinfection promotes escape mutations. Our simulations suggest that adaptive vaccination programs, requiring adequate strain and serology monitoring and surveillance, are needed to extirpate outbreaks. Our platform provides policymakers with an easy-to-use tool for designing effective vaccination programs. Our RAMP concept points the way to the development of highly flexible models that are easily shared among researchers and policymakers in all areas of systems analysis.

medRxiv preprint doi: https://doi.org/10.1101/2021.06.07.21258504; this version posted June 11, 2021. The copyright holder for this preprint (which was not certified by peer review) is the author/funder, who has granted medRxiv a license to display the preprint in perpetuity. All rights reserved. No reuse allowed without permission.

Introduction

Vaccines have either eliminated, or all but eliminated, diptheria, measles, polio, rubella, small pox, and tetanus within developed countries, such as the USA [1]. The global COVID-19 pandemic has amply illustrated the overwhelming economic importance that vaccines can play in bringing an epidemic under control [2]. Unlike the above mentioned diseases and more inline with influenza, however, the SARS-CoV-2 pathogen may re-emerge with vengeance due both to waning immunity and proliferation of mutant strains or variants with increased transmissibility that escape both naturally-acquired and vaccine-induced immunity [3–8]. To investigate how effective vaccination programs may be in preventing future large-scale outbreaks of COVID-19 [9, 10], we built a Java Runtime-Alterable-Model Platform (J-RAMP) of an SEIVD (Susceptible, Exposed, Infectious, V=Immune & Vaccinated, Dead) individual-based model (IBM) [11–14] that includes the following processes (Fig. 1; see Materials and Methods, as well as Appendix A for details):

- pathogen strain-specific shedding [15], environmental persistence [16], with-host replication [17] and mortality rates [18] (some prefer the term variant rather than strain)
- immunological waning with strain cross immunity [6, 19]
- pathogen strain drift during transmission and within-host replication [20]
- an adaptive contact rate [21]
- a time-dependent, uni- or multivalent vaccine rollout [22, 23]

Our SEIVD-IBM J-RAMP, is an example of our novel runtime alterable-model platform (RAMP) concept, which includes panels, windows and sliders that allow users to specify and manipulate model parameter values in real time, as well as modify process function descriptions, even during the course of a simulation, while protecting the integrity of the underlying code. Thus our SEIVD-IBM J-RAMP has epidemiological applications well beyond COVID-19, including diseases such as influenza [24], Ebola [25, 26], and any other directly transmitted disease [27]. To illustrate its application, we used our J-RAMP to explore the relative efficacy of uni- and multivalent vaccines applied at various time-dependent rates, where choice of valency may switch in response to realtime monitoring and surveillance data. Such adaptive vaccination programs may be required to combat the evolutionary arms race between vaccine efficacy and the evolution of new pathogen strains [20, 23, 28]. We demonstrate the possible consequences of vaccinating too few individuals in the context of the emergence of more transmissible strains, as well as the comparative efficacy of non-adapative versus adaptive vaccines responsive in realtime to current strain valency. We simulate plausible COVID-19 outbreaks over a three year period in which vaccination rollout commences at the start of year two and continues until the end of the year three.

Our study is meant to highlight issues related to vaccination rollout rates [10] and strain valency that may turn out to provide insufficient coverage of the population or being outrun by waning immunity in vaccinated hosts or those that have survived COVID-19. We undertake these simulation with the knowledge that though a typical set of parameters may cover most outbreaks of COVID-19

medRxiv preprint doi: https://doi.org/10.1101/2021.06.07.21258504; this version posted June 11, 2021. The copyright holder for this preprint (which was not certified by peer review) is the author/funder, who has granted medRxiv a license to display the preprint in perpetuity. All rights reserved. No reuse allowed without permission.

in various regions around the world, regional differences in the contact behavior of individuals, with additional contact rate time dependency in each locality due to social distancing regulations and behavior, have led to markedly different outbreak patterns across regions [29–31]. Thus the result presented here are meant to inform us of potential pitfalls and dangers in rolling out inadequate vaccination programs and extract general principles, where possible, as well as illustrate an approach to its local application rather than prescribe a universal program: adaptive programs need to operate in response to local surveillance data and contact rate conditions.

The local nature of contact rate patterns is well established as an important driver of outbreak patterns [30]. The definition of a contact where transmission may occur is rather challenging though. Effective or "close" contact may be defined, as in [32], in terms of direct physical contact or close conversation, or it may involve concepts of a threshold distance and time period [33]. Taken a step further, it may relate to infectious dose levels and the relationship between dose and severity of the infection of individuals [34]. This effective contact rate issue, however, is side-stepped by fitting models to local incidence data to obtain a concatenated contact-and-transmission rate parameter value that best fits local outbreak patterns, as discussed in depth elsewhere [30].

Our results also suggest that adaptive vaccination programs that closely monitor the emergence of new strains and adapt vaccine valency to match predominating strains are much more likely to extirpate local epidemics than non-adaptive policies, though our simulation results are greatly influenced by assumptions regarding rates of waning immunity and strain cross-immunity characteristics as well. Accurate forecasting of the future course of an epidemic in terms of strain composition and vaccination program efficacy require data on the rates at which immunity wanes, how such immunity depends on particular strains, and the levels of cross immunity among strains [4, 6] that are more comprehensive than currently available. It also requires better data on within-host replication and mutation rates. Thus, in truth, we present our model and results fully aware that answers to questions relating the design of optimal region-specific vaccination programs await more reliable data on immunity processes, strain mutation rates [35], and the transmission potential and virulence of dominant strains [36]. We hope, however, that our results and subsequent investigations using our model provide the kinds of quantitative analyses that can help formulate highly effective local or country level vaccination programs that avoid many of the pitfalls revealed by our analysis, as well as encourage the adoption of rapidly adaptive vaccination programs.

Results

Single strain simulations

Our first simulation, which we regard as a "baseline run" has $J = 0$ (i.e., only one strain is possible), assumes a constant contact rate ($\kappa(t) = \kappa_0$ for all t; which implies no social distancing or effective contact reducing actions taken) in an a homogeneously, well-mixed population of ten thousand individuals ($N_0 = 10,000$), with an immune waning half-life of one year ($t^{\text{half}} = 365$), and no vaccination rollout. The resulting simulation depicts a classic outbreak pattern

medRxiv preprint doi: https://doi.org/10.1101/2021.06.07.21258504; this version posted June 11, 2021. The copyright holder for this preprint (which was not certified by peer review) is the author/funder, who has granted medRxiv a license to display the preprint in perpetuity. All rights reserved. No reuse allowed without permission.

(Fig. 2) in which incidence rises to a peak of about 250 cases around 96 days after "patient zero" has been introduced, and then burns out around day 166 days because an insufficient number of susceptible individuals are now available to keep the epidemic going. In the upper left-hand panel of our SEIVD-IBM J-RAMP dashboard in Fig. 2, we see that around 3/4 of individuals have been infected at the point where the epidemic burns out ($V(166) = 7700$, which is 77% of N_0): this suggests that herd immunity may well be in the ball park of 75-80% (as supported by additional runs presented next), although this would be an underestimate if more transmissible strains come to prevail.

Repeated runs of this first simulation with different runtime seeds (viz., 10 runs with runtime seeds ranging from 0 to , where each seed generates its own, essentially unique, but repeatedly sequence of pseudo random numbers; Fig. 2 is for the case runtime seed = 0) produces the following means and standard deviations as a percentage of the population size (of S, V and D), as well as the length of the epidemic (days) (see Fig. C.1, Appendix C): $S_{\text{fnl}} = 21.9 \pm 0.6\%$, $V_{\text{fnl}} = 76.4 \pm 0.6\%$, $D_{\text{fnl}} = 1.6 \pm 0.1\%$, and $t_{\text{fnl}} = 167 \pm 9$ days. These results are almost the same when the initial population size is increased threefold to $N_0 = 30,000$ individuals, the primary difference being a small expected decrease in variability (around $1/3^{\text{rd}}$ smaller) and slightly longer epidemic period (18% longer) (see Fig. C.1 for details). To obtain full plots of the incidence, prevalence, and daily-death trajectories from many runs of our SEIV-IBM, we exploited the R-platform integrability of our J-RAMP to generate mean and standard deviation plots of incidence, prevalence, and daily mortality, as described in Appendix B (and Fig. C.2).

Our second single-strain ($J = 0$) simulation (Fig. 3A) illustrates that, for the selected set of parameter values, if the rate of waning is tripled from that of our first (i.e., t^{half} is reduced from 365 days to 120 days) then herd immunity is still reached. Our third single strain simulation, however, shows that herd immunity is eluded for the selected set of parameter values when this rate is quadrupled ($t^{\text{half}} = 90$ days; Fig. 3B): viz., the population enters a periodic outbreak mode because previously infected individuals are sufficiently susceptible after several months post-initial infection to be reinfected and thus keep the epidemic going. Herd immunity in this caricatured population (i.e., relatively small, isolated, homogeneous) would also be reached within a year if the waning immunity half-life is increased back to $t^{\text{half}} = 180$, but not if an adaptive contact rate is in operation (Fig. 3C & D; $k(t)$ specified by Eq. A.10). More specifically, for the case $p_{\text{I}}^{\text{half}} = 0.05$, that is the "effective" contact rate $\kappa(t)$ drops from $\kappa(t) = \kappa_0 = 4$ when $I/N_0 = 0$ to $\kappa(t) = \kappa_0/2 = 2$ when $I(t)/N(t) = 0.05$, our fourth single strain simulation indicates that prevalence peaks at roughly 400 individuals (i.e., just around 0.4% of the population) around day 85 (Fig. 3C), drops to around 50 between days 210 and 240, and then rises back to over 200 by the end of one year. In our fifth single strain simulation (Fig. 3D), an additional 5-fold reduction in our adaptive contact rate (i.e., $\kappa(t) = \kappa_0/2 = 2$ when $I(t)/N(t) = 0.01$) produces a prevalence of just under 100/10,000=0.01% that appears to persist with stochastic noise from day 100 onwards.

We carried out two additional single strain simulations, this time for three years, and applied a vaccination rollout program that vaccinated individuals drawn at random in the second and third year at rates $v = 0.001$ and $v =$

medRxiv preprint doi: https://doi.org/10.1101/2021.06.07.21258504; this version posted June 11, 2021. The copyright holder for this preprint (which was not certified by peer review) is the author/funder, who has granted medRxiv a license to display the preprint in perpetuity. All rights reserved. No reuse allowed without permission.

0.002 (0.1% and 0.2% of the population vaccinated each day; Fig. 4A & B), respectively, from a pool consisting of individuals not currently infectious or previously vaccinated. In these runs, we set $t^{\text{half}} = 365$ days, $p_{\text{I}}^{\text{half}} = 0.002$ (reflecting US case percentages after 1 year), with a population size of $N_0 = 100,000$. In the case $v = 0.001$, the vaccination rate was insufficient to overcome the rate at which infected individuals were becoming reinfected due to waning immunity. In the case $v = 0.002$, the vaccination rate was sufficiently high to bring the epidemic under control. In the latter case, however, if we no longer allow individuals who had previously been infected to be part of the vaccination pool as well (i.e. we confine vaccinations to the **S** class only), the vaccination rollout rate $v = 0.002$ is now insufficient to extinguish the outbreak and a resurgence occurs around the end of the second year (Fig. 4C).

Multi-strain simulations

In all our multi-strain simulations we set $p_{\text{I}}^{\text{half}} = 0.005$. This latter value, as previously mentioned, produces a cumulative number of cases of around 10% in the first year in a population of size $N_0 = 100,000$ (Appendix C, Fig. C.3), which is in the ballpark of 8.5% for the US outbreak during its first year.

In our first set of multistrain simulations, we set $J = 4$ (i.e., permitting 16 strains) and compared the situations where cross immunity is absent ($c = 0$; Fig. 5A) to where it has the intermediate value $c = 0.5$ (Fig. 5B). The remaining parameters were the same for all strains and used the same basic epidemiological parameters, as in our previous single strain simulations, although mutation rates were now added to enable new strains to proliferate (see caption to Fig. 5 for details on parameter values).

In the no cross immunity (Fig. 5A) case, we see that the initial surge is driven by strain $0 \equiv (0,0,0,0)$ (see discussion in Appendix A for use of binary representation), which is first replaced by strain $8 \equiv (1,0,0,0)$ around the end of year 1, which in turn is somewhat displaced by strains $7 \equiv (0,1,1,1)$ and $6 \equiv (0,1,1,0)$, with strain $1 \equiv (0,0,0,1)$ coming to dominate at the start of year 3, only to be finally challenged by strain $3 \equiv (0,0,1,1)$ towards the end of year 3. In the nearest-neighbor cross immunity case (Fig. 5B), given the retarding effect of cross immunity on the proliferation of strains that differ in only one allele from the initial dominating strain $0 \equiv (0,0,0,0)$, this initial strain was displaced by strains $3 \equiv (0,0,1,1)$ and $11 \equiv (1,0,1,1)$ around the end of year 1. These latter 2 strains were then displaced by strain $7 \equiv (0,1,1,0)$ during the first half of year 3, with strain $13 \equiv (1,1,0,1)$ dominating at the end of year 3 somewhat supported at a lower level by strain $14 \equiv (1,1,1,0)$. We also noticed a moderate resurgence of strain $0 \equiv (0,0,0,0)$ in the middle of year 3.

In a second set of multistrain simulations, we set $J = 7$ for a total of 128 possible strains. Unlike the previous set of multistrain simulations, we now provided a strain specific set of transmission parameters $\bar{\beta}_j$ by selecting these at random on the interval $[0, 0.3]$, apart from a dominant sequence of transmission values that steps in increments of 0.25 from 0.3 in strain 0 to 0.475 in strain 127 along the sequence mentioned in the caption to Fig. 6 and documented in Fig. C.4. The remaining parameters are the same as for the simulation depicted in Fig. 5B (i.e., the cross-immunity parameter $c = 0.5$). Unlike the

medRxiv preprint doi: https://doi.org/10.1101/2021.06.07.21258504; this version posted June 11, 2021. The copyright holder for this preprint (which was not certified by peer review) is the author/funder, who has granted medRxiv a license to display the preprint in perpetuity. All rights reserved. No reuse allowed without permission.

case, $J = 4$, only two strains now played any serious role in the outbreak in the non-vaccination scenario (Fig. 6A): strain $0 \equiv (0,0,0,0,0,0,0)$ for the first year and strain $127 \equiv (1,1,1,1,1,1,1)$, the most transmissible, for the remaining 2 years.

Vaccination rollout simulations

Following our no-vaccination simulation of our 128-strain case (Case A; Fig. 6A), we explored three different vaccination rollout programs applied in years 2 and 3 with the following vaccination rates and vaccine strain valencies: Case B, rate $v = 0.002$ (i.e., 0.2% vaccinated per day), strain valency 0 (Fig. 6B); Case C, rate $v = 0.002$, strain valency 127 (Fig. 6C); and Case D, $v = 0.01$, strain valency (0,7,31,127) (Fig. 6D). Each of these vaccination programs begin with the initial strain $0 \equiv (0,0,0,0,0,0,0)$ being replaced by strain $127 \equiv (1,1,1,1,1,1,1)$ towards the end of year 1 or start of year 2.

Alarmingly, the first vaccination rollout scenario (Case B) made the epidemic worse rather than better when compared with the no vaccination scenario (number of deaths were 1366 versus 1122; compare Figs. 6A and B) because the vaccination rollout with its strain 0 valence vaccine, though delaying the emergence of strain 127, led to an increased prevalence of this most transmissible strain ($\beta_{127} = 0.475$ versus $\beta_0 = 0.300$). Using a strain 127 valence vaccination (Case C) had some effect in reducing the 3-year death total back to 1109, but the efficacy of this rollout was thwarted by the emergence of strain $48 \equiv (0,1,1,0,0,0,0)$ ($\beta_{48} = 0.295$, Fig. 6C).

Given the inability of these two monovalent vaccination rollout programs in years 2 and 3 to control the outbreak, we simulated the much more aggressive rollout program of a quadravalent (0,7,31,127) vaccine applied at a rate of 1% per day ($v = 0.01$; a five-fold increase over the previous two monovalent programs) in a system with increased levels of cross immunity (cascading versus simple) and including revaccination of previously vaccinated individuals to combat the effects of waning immunity. Even this aggressive vaccination rollout program failed, although it did knock the incidence way down at the start of the rollout. The efficacy of this rollout, however, was thwarted by the rise of strain $23 \equiv (0,0,1,0,1,1,1)$ ($\beta_{23} = 0.214$) during the mid to latter part of the second year, which was then supplanted by strain $3 \equiv (0,0,0,0,0,1,1)$ ($\beta_3 = 0.350$), which dominated the third year (Fig. 6D).

Unsurprisingly, the success of any vaccination program depends on the relative robustness of the immunity characteristics of hosts to the various strains. Thus, in regard to the vaccination programs represented by cases **B** and **C** (Fig. 6, we simulated the rollout of a bivalent vaccine with strain valency (0,127) implemented at the same vaccination rate of $v = 0.002$, but in a system with much more robust immunity characteristics: a waning half-life increased from $t^{\text{half}} = 365$ to 1825 days (a five-fold increase) and a cascading cross immunity system with c increased from 0.5 to 0.9. In this case, the outbreak was rapidly extirpated after 257 days (i.e., from start at day 365 to extirpation at day 622).

Given the failure of our first three 128 strain vaccination rollouts (cases **B** to **D** in Fig. 6) to extirpate the simulated epidemics, we investigated whether rollout programs that adapted vaccine valencies to track in real time the emer-

medRxiv preprint doi: https://doi.org/10.1101/2021.06.07.21258504; this version posted June 11, 2021. The copyright holder for this preprint (which was not certified by peer review) is the author/funder, who has granted medRxiv a license to display the preprint in perpetuity. All rights reserved. No reuse allowed without permission.

gence of dominant strains might be more effective. Thus, we used a JS scripting window to write a JavaScript driver (as described in Appendix B; see Fig. B.4) that adapted (i.e., switched as necessary) the valency of the vaccine every 90 days after the start of the vaccination rollout to match the top two strains prevalent at time of switching, or only the top strain if no other strain exceeded a prevalence of 10 individuals. The results of these two simulations, one for the nearest-neighbor cross-immunity case (Eq. 1) and one for the cascading cross-immunity case (Eq. A.7), are provided in Fig. 7. They should be compared with the non-vaccination case depicted in Fig. 6A and the non adaptive vaccination rollout depicted in Fig. 6D. In contrast with the latter—and despite having the same vaccination rates, the same strategies for selecting non-infected individuals at random, and employing vaccines with fewer strain valency—both of these adaptive vaccination rollouts extirpated the epidemic, the first within half a year (Case A) and the second within 1.4 years (Case B) from the start of vaccination rollout.

Discussion

The amount of structure and data needed in complex biological systems' models, depends on the questions that these models have been formulated to address [26,37]. In this paper, we steered away from making specific predictions—because universal solutions are not always locally applicable. Rather, we focused on questions relating to the potential efficacy of different vaccination rollouts (both vaccination rates and valencies of vaccines) in the context of strain emergence and the potential for vaccination programs to go awry. To make specific predictions requires localized data, particularly as it may relate to social distancing behavior or other factors that affect contact rates over time [30, 38, 39]. Additionally, we cannot expect models to make strain-specific informative predictions, unless they have been designed to do so and are supported by location specific data regarding the relative transmissibility of strains and other strain specific data. In the absence of such data, models become a tool for anticipating pitfalls and avoiding unintended consequences of well-intentioned actions. Equally important, however, is the implementation of our model as a RAMP (runtime alterable model platform), because this greatly facilitates the use of our model by ourselves and others in testing out different hypothesis about the process generating observed population level strain transmission dynamics.

The illustrative simulations we present demonstrate that if vaccination rollout rates and vaccine valencies are applied in blanket manner—that is, without monitoring strain emergence and obtaining some assessment of the epidemiological characteristics of those strains (e.g., relative transmissibility, virulence, waning and cross immunity characteristics)—then the possibility exists for a vaccination program to do more harm than good. This of course, is not to say that vaccination programs should ever be avoided; only that once a vaccination program is embarked upon, it should be implemented at a sufficiently vigorous rate to ensure that it is not outrun by relatively fast waning immunity rates. Additionally, when escape mutations emerge, generally associated with reinfection cases [8], then the valency of vaccines should be switched rapidly enough to

medRxiv preprint doi: https://doi.org/10.1101/2021.06.07.21258504; this version posted June 11, 2021. The copyright holder for this preprint (which was not certified by peer review) is the author/funder, who has granted medRxiv a license to display the preprint in perpetuity. All rights reserved. No reuse allowed without permission.

thwart escape mutations, rather than aiding such mutations by thwarting less transmissible competing strains instead.

At this time, the primary value of our SEIVD-IBM J-RAMP is in testing various vaccination strategies as they relate to strain emergence [40] and identifying pitfalls related to the unintended promotion of more transmissible or virulent strains. Strain emergence has both a local and global component. Particular strains may first be identified as occurring in specific geographical regions, as in the strains that appear to have originated in the UK (B.1.7.7 variant), South Africa (variants B.1.1.54, B.1.1.56 and the C.1 lineage) and Brazil (P.1 lineage) [41]. Thus more geographically focused application of our J-RAMP may require more specific strain related information. Such information would then be used to get estimates of the relative values of transmissibility β_j, virulence α_j, and even of shedding ($\bar{\zeta}_{jm}$) and environmental persistence ($\bar{\eta}_j$). But equally important in evaluating the impacts of vaccination strategies on local outbreaks is obtaining strain-specific cross-immunity data (for characterization of the elements $c_{j\ell}$ of the cross immunity matrix $\mathbf{C}$), waning rates (which we have not made strain specific, but our model could be generalized to include strain specific values t_j^{half}), and the relative within host competition values (i.e., λ_j, which we have set all equal to 1 at this time in the absence of data to the contrary). Models are sorely needed to explore multistrain dynamics, particularly the epidemiological properties with regard to shedding, environmental persistence, transmission, mutation, and within-host replication rates, which acting together determine the relative success of different strains and their actual impact on the severity of epidemics and the nature of vaccination programs needed to suppress them.

The process of making our model both location and strain specific could be undertaken using methods designed to enhance the relevancy of models, such as Appropriate Complexity Modeling (ACM: [26,37]). Further, in some cases it may be useful to add spatial or age-structure information to our SEIVD model IBMs or include a contact network [42], which itself may contain spatial or refined class category (e.g. age or work category) information. In addition, our current implementation represents strain differences in terms of J loci with two alleles (denoted by 0 and 1 respectively) at each locus. A more realistic representation of the genetic basis of strain differences may involve a more involved genetic representation in which several alleles are possible at each locus.

Although cross-immunity and immune waning are entangled in our immunity modifier functions (i.e., ϕ_{ij} ; see Eq. A.11), cross-neutralization data can be used to estimate the cross and waning immunity parameters using appropriate methods [43,44]. Such data are becoming more widely available through the application of rapid PCR methods [3,45,46]. Strain or variant cross neutralizing studies bring up a much neglected issue, which is the effect of dose (number of pathogens involved in the initial infection, also know as viral load) on the severity of the infection. This differs from the questions of the number of doses—usually one or two—constituting and vaccine regimen versus the viral load (or antigen load, or virus-like particle load when only antigens or parts of viruses are administered) in each dose [4]. In the context of vaccination, both these issues and the technology used to produce the vaccine [23] may well have an impact on waning immunity half-lives and cross-immunity values. Thus,

medRxiv preprint doi: https://doi.org/10.1101/2021.06.07.21258504; this version posted June 11, 2021. The copyright holder for this preprint (which was not certified by peer review) is the author/funder, who has granted medRxiv a license to display the preprint in perpetuity. All rights reserved. No reuse allowed without permission.

the parameter values used in the model should ultimately be vaccine specific. Further, when it comes to determining waning and cross immunity parameter values, our model does not distinguish between individuals that have been infected with a particular strain or vaccinated with a valency related to that strain.

In the coming year, as we obtain more information on the nature of immunity to SARS-CoV-2, it will become more apparent to us whether or not COVID-19 will settle into global endemicity [19, 47]. If this is the case, then constant vigilance and a well designed vaccination program with respect to vaccinating the young and implementing booster vaccinations with appropriate strain valency will become the order of the day. The J-RAMP presented here, with appropriate elaborations that will become evident through its future application, such as being able to compute the best time to administer booster shots of the same or different strain valencies to individuals, should play a decisive role in the rational design of effective and efficient COVID-19 vaccination programs worldwide. This is made apparent from the simulations we present here that, depending on the immunological characteristics of hosts and mutational rates of SARS-Cov-2, it may be harder than currently anticipated to extinguish COVID-19 in the next few years through non-adaptive vaccination programs. Thus, we should endeavor to adapt the strain valency of our vaccines as rapidly as possible to the predominating SARS-Cov-2 strains, identified from ongoing monitoring and surveillance programs.

Finally, the concept of runtime-alterable, modeling platforms (RAMPs), with driver script and other coding platform integration, in our case developed in Java with R platform integration and a JavaScript simulation driver window, provides the first example of a new concept in model implementation that facilitates model sharing and easy modification by users other than the original developers. We believe such platforms can come to play an important role not only in disease modeling, but in all fields of research that rely on models for comprehensive analyses of the behavior of systems of interest.

Materials and Methods

Our SEIVD-IBM in a nutshell

We constructed an individual-based model (IBM) of a susceptible-exposed-infectious-recovered (i.e., an SEIVD model, where removed R are split into V=immune/vaccinated, and D=dead) epidemiological process [11, 12] in a homogeneous population with a random encounter contact rate parameter $\kappa_0 > 0$. Our formulation includes a host immunological waning process [6, 19]. It also includes the emergence of pathogen strains due to a mutational process that impacts both transmission of mutant strains from the infectee and genetic drift [3, 5, 48] of strains within the infector, with rates impacted by cross immunity effects. We allowed for variation in pathogen strain transmissibility (i.e., in the $\beta > 0$ parameter of the frequency dependent transmission function $\beta SI/N$ [49, 50]) and pathogen virulence as represented by the disease-induced host mortality rate sensu Anderson and May [51] (and often represented by a parameter $\alpha \geq 0$ [49]).

medRxiv preprint doi: https://doi.org/10.1101/2021.06.07.21258504; this version posted June 11, 2021. The copyright holder for this preprint (which was not certified by peer review) is the author/funder, who has granted medRxiv a license to display the preprint in perpetuity. All rights reserved. No reuse allowed without permission.

The detailed formulation of our model and its algorithmic implementation is provided in Appendix A. In a nutshell we:

1. defined a set of 2^J pathogen strains (user selected value for J ranging from 0 to 8; pathogen index $j = 0, ..., 2^J - 1$) with a genetic-relatedness topology of a J-dimensional unit cube—i.e., each pathogen has J-loci that can take on one of two allelic values at each locus with immediate neighboring strains differing from each other by exactly one allelic value (0 or 1) at only one of the J loci
2. defined a population of N_0 hosts as belonging at time t to either an epidemiologically naïve set of susceptible individuals $\mathbf{S}$ of size $N_{\mathrm{S}}(t)$, a set $\mathbf{A}$ of $N_{\mathrm{A}}(t)$ identified agents A_i $(i = 1, ..., N_{\mathrm{A}}(t))$ whose epidemiological histories are known, or a set $\mathbf{D}$ of $N_{\mathrm{D}}(t)$ individuals that have died from the disease
3. allow pathogen strain-specific transmission "force" $(\bar{\beta}_j > 0)$ and virulence $(\alpha_j \geq 0)$ parameters to vary in value among one another within a defined range $\bar{\beta}_j \in [\beta_{\min}, \beta_{\max}]$ and $\alpha_j \in [\alpha_{\min}, \alpha_{\max}]$
4. kept track of the total prevalence N_{I} as the sum of the prevalences of the individual strains N_{I_j}, $j = 0, ..., 2^J - 1$—i.e. $N_{\mathrm{I}} = \sum_{j=0}^{2^J-1} N_{\mathrm{I}_j}$
5. introduced a random contact rate function $\kappa(t)$ with a constant parameter κ_0 that is Poisson distributed on $[t, t+1)$, $t = 0, 1, \cdots$, multiplied by an adaptive response function that reduces the contact rate with increasing disease prevalence, such that the $\kappa(t)$ is reduced to $\kappa_0/2$ when the $N_{\mathrm{I}}(t)/(N_0 - N_{\mathrm{D}}) = p_{\mathrm{I}}^{\mathrm{half}}$—see Eq. A.10 in Appendix A
6. update the epidemiological state of the agents A_i with respect to each of the strains $j = 0, ..., 2^J - 1$ where the state with respect to particular strain j at time t is represented by
   (a) 0: has never been infected with this strain
   (b) $\mathrm{E}_j(t, \tau_{ij})$: infected at time $\tau_{ij} \leq t$ with this strain, but not yet infectious for an expected period of σ_{E} units of time
   (c) $\mathrm{I}_j(t, \tau_{ij})$: infectious at time t with this strain, for an expected period of σ_{I} units of time, having been most recently infected (reinfections with the same strain may occur) with this strain at time $\tau_{ij} < t$
   (d) $\mathrm{V}_j(t, \tau_{ij})$: has now recovered from its most recent infection at time τ_{ij} with this strain and has some level of waning immunity to it

   where we assume that agent A_i can be infected at time t with at most one dominant strain (denoted by the index j), although it will have different levels of waning immunity to all of the strains to which it has been infected in the past
7. included waning immunity functions $\omega_{ij}(t)$ (symbol is omega: Eq. A.6) used to compute the level of immunity that agent A_i has to its most recent infection by strain j
8. included cross immunity constraints (a J^2-matrix C) that apply both to the *infector* transmitting the pathogen and the *infectee* being invaded (inv) by the pathogen, both of which reduce the likelihood of infection and strain drift by strain j compared with closely related strains ℓ
9. computed an *infection probability* $\pi_{ih,j\ell}^{\mathrm{inf}}$ that agent A_i infected with strain j infects agent A_h with strain ℓ in terms of a concatenation of infector viral shedding $(\zeta_{i\ell})$, viral persistence in the environment (ε_ℓ), and viral transmission $(\beta_{h\ell})$ processes (Fig. 1)

medRxiv preprint doi: https://doi.org/10.1101/2021.06.07.21258504; this version posted June 11, 2021. The copyright holder for this preprint (which was not certified by peer review) is the author/funder, who has granted medRxiv a license to display the preprint in perpetuity. All rights reserved. No reuse allowed without permission.

10. computed an *invasion probability* $\pi^{\text{inv}}_{h\ell\ell'}$ that an agent A_h infected with strain ℓ becomes infectious with strain ℓ' as its major strain, in terms of the multiplicative effects of viral mutation (μ) and viral replication (λ_ℓ) processes ongoing within an infectee A_h during this infectees exposed ($\mathrm{E}_{\ell'\tau_{h\ell'}}$) and infectious ($\mathrm{I}_{\ell'\tau_{h\ell'}}$) stages (Fig. 1)
11. computed the overall probability $\pi_{ih,j\ell'}$ that that an infector A_i infected with major strain j results in an infectee A_h expressing ℓ' as its major strain
12. implemented a discrete time individual-based stochastic SEIVD (here V represents individuals that have either recovered from infection or have been vaccinated, D represents cumulative dead) multi-strain model that includes specifiable time-dependent univalent and multivalent vaccination applications

Our J-RAMP implementation

Models of systems process can be coded as singular implementations model formulations using: i) highly efficiently compilable computer languages (e.g., C++, FORTRAN, Java) ; or ii) less efficiently, but more easily coded, scriptable (e.g., JavaScript, Python, Perl) computer languages. More conveniently and expeditiously, they can be coded up, as discussed in [52], using a systems modeling platform, such as Matlab's SIMULINK, Mathematica, Stella, AnyLogic, Numerus, or Berkeley Madonna. Advantages of the latter include more rapid and accurate model development, though simulations may be slowed down by platform overhead. Between these extremes, we propose a more general approach to specific classes of systems' models, where the basic system structure is fixed, but implementation of some elements can be easily and safely altered so that optional implementations are presented at runtime. We call such a design *runtime alterable-model platforms*. (RAMPs); and here we present a Java RAMP implementation of the SEIVD-IBM described in the previous subsection.

medRxiv preprint doi: https://doi.org/10.1101/2021.06.07.21258504; this version posted June 11, 2021. The copyright holder for this preprint (which was not certified by peer review) is the author/funder, who has granted medRxiv a license to display the preprint in perpetuity. All rights reserved. No reuse allowed without permission.

The characteristics we envision for a model platform to be a RAMP are:

1. RAMPs include a set of model parameters (constants) whose values can be selected or specified (sometimes within a predefined range of values) at simulation runtime using a switch, nob, slider, or text-entry window accessed via a platform graphical interface or dashboard (e.g., see Fig. 2 and Table 1 which apply to our SEIVD-IBM J-RAMP).
2. RAMPs include a specific set of *runtime alternative modules*, (RAMs), where the original can be redefined in a graphical interface window, and the unaltered original and the alternative routines are stored as a (preferably open-ended) numbered set. The original or any one of the alternatives can be selected for use at runtime (for a list of functions in our RAMP see Table 2).
3. RAMP implementations also provide an API for both remote and on-board scripting. This API enables control of all user aspects of the simulation, including the parameter set, run management, RAM options, and data retrieval. Script logic can alter parameter settings and RAM options as the simulation progresses. A Nashorn-based Javascript interpreter enhanced with API methods is provided.
4. The API can be accessed remotely using operating system facilities by external applications running concurrently with the simulator. Of particular interest is the ability to control the simulation from the R statistical platform. An R routine can be formulated to both manage the simulation run and to retrieve and process the resulting data. The RAMP simulation becomes a "virtual package" to the controlling R logic. See Appendix B.

We implemented our RAMP using Java and made ample use of all of the features described above. Use of the RAM facility permitted experimentation with the several versions of cross immunity presented in this paper. A Javascript program was used to control an adaptive vaccination strategy. A small R package serving as a driver was used in an R program that ran the simulation multiple times, extracted results into R data structures, and produced graphs showing statistical mean and standard deviation. More details on the graphical structure and implementation of our SEIVD-IBM are both implied in the presentation of results below, and in additional details provided in Appendix B.

COVID-19 model assumptions and parameter values

The first variable that needs to be determined is the unit of time we use for our simulations because all process rate parameters are scaled by its selection. Since the time resolution of empirical COVID-19 incidence and mortality data is daily, we selected are unit of time t to be days. Additionally, based on various sources including a metapopulation study of COVID-19 parameter estimates [53], we set the latent and infectious periods to be 4 and 7 days respectively. Basic SEIR epidemiological models do not separate out the processes of contact and transmission-per-contact, so we had some leeway on what values to choose for contact rates and transmission rates per contact because it is the value of the product of these that is important in determining the reproductive value, commonly referred to as "R_0" for COVID-19. Hussein et al.'s [53] meta analysis of COVID-19 zeroed in on $R_0 = 3.14$ as a mean value across a range of studies

medRxiv preprint doi: https://doi.org/10.1101/2021.06.07.21258504; this version posted June 11, 2021. The copyright holder for this preprint (which was not certified by peer review) is the author/funder, who has granted medRxiv a license to display the preprint in perpetuity. All rights reserved. No reuse allowed without permission.

(95% confidence interval $[2.69, 3.59]$) though these authors suggested that the most recent studies they looked at suggested that R_0 was more likely between 2 and 3.

Assuming no seasonal effects (i.e., $\delta = 0$ in Eq. 3), in our single strain runs we kept $R_0 \approx 3$ by setting $\kappa = 4$ (effective contacts per day, which nominally involves being with 6 feet of one another at least 15 mins) thereby requiring $\beta = 0.3$, because in the notation of the continuous time model introduced in Eq. A.29, we have an inverse latent period value of $\gamma \equiv 1/\sigma_{\mathrm{E}} = 1/4$ and an inverse infectious period value of $\rho \equiv 1/\sigma_{\mathrm{I}} = 1/7$ days (Table 1) for Eq. A.29 to yield $R_0 = \frac{4\times 0.3}{1/4+1/7} = 3.05$

In our multistrain runs, we did allow for the emergence of strains that were more transmissible than this single strain value (in these runs new strains were in the range [0,0.475] (see table depicted in Fig. C.4). Also, although the incubation period is typically thought to have a median of 5 days, it can be much faster [54].

In reality, the contact rate κ is not constant, but is time varying. It is influenced by the social distancing behavior of individuals who may be responding to fears of contracting the disease, or regulations imposed by local authorities to reduce effective contact rates. To account for this, we formulated an adaptive contact rate function $\kappa(t)$ (Eq. A.10) in terms of a function that declines adaptively from a non-epidemic (baseline maximum) value κ_0 to $\kappa_0/2$ when the prevalence (the percentage of the population infectious at time t) increases to $\frac{N_{\mathrm{I}}(t)}{N(t)-N_{\mathrm{D}}(t)} = p_{\mathrm{I}}^{\mathrm{half}}$. In the illustrative simulations presented here, we explore the effect of varying $p_{\mathrm{I}}^{\mathrm{half}}$ on the size of the shape of epidemic, but set $p_{\mathrm{I}}^{\mathrm{half}} = 0.002$ (i.e., a prevalence level of 0.2%) as a baseline value, because in our simulations this baseline value, along with the parameter values selected above, results in a cumulative number of cases to just over 11% in a population of $N = 100,000$ (Appendix C, Fig. C.3). This puts our illustrative baseline case in the ballpark of the US outbreak which Worldometer reported to have a cumulative case level of 8.5% ($\approx 284.5 \times 10^6/332.9 \times 10^6$) after one year, but this is likely to be a substantial underestimate of the actual number of cases [55].

To keep things simple in applying our model to a multistrain setting, we assumed that the immune effects on infector shedding and mutation and replication within the infectee through a cross-immunity processes, can be tweaked through a single constant $c \in [0, 1)$ (making the elements $c_{j\ell}$ of the matrix C strain-dependent will obviously require considerable supporting data). One scenario is to assume cross immunity only applies to nearest neighbors, i.e.:

$$\text{Nearest-neighbor } \mathbf{C}: \qquad c_{j\ell} = \begin{cases} 1 & \text{if } \ell = j \\ c & \text{if } \ell \text{ differs from } j \text{ by one allele} \\ 0 & \text{otherwise} \end{cases} \tag{1}$$

For other formulations, such as "Cascading **C**" or including escape mutations in the mix see Eqs. A.7 and A.9 in Appendix A.

Additionally, we expect this type of evidence to become increasing available with whole genome sequence of pathogen strains [56] collected during host shedding. For simplicity's sake, however, we assume that infectee with major strain j will shed minor strains in the immediate neighborhood of j at comparative

medRxiv preprint doi: https://doi.org/10.1101/2021.06.07.21258504; this version posted June 11, 2021. The copyright holder for this preprint (which was not certified by peer review) is the author/funder, who has granted medRxiv a license to display the preprint in perpetuity. All rights reserved. No reuse allowed without permission.

rate $\zeta \in [0, 1)$ and be major strain-independent: i.e., we assume

$$\zeta_{j\ell} = \begin{cases} 1 & \text{if } \ell = j \\ \zeta & \text{if } \ell \text{ differs from } j \text{ by one allele} \\ 0 & \text{otherwise} \end{cases} \tag{2}$$

Third, again in the absence of evidence to the contrary, we assume that seasonal fluctuations are strain independent. In this case, for strain-independent constants $\delta \in [0, 1)$ and $\theta \in [-\pi, \pi]$ that set seasonal fluctuations related to environmental persistence, Eq. A.13 in the Appendix A simplifies for a single constant $\bar{\eta}$ to:

$$\eta_\ell(t) = \bar{\eta}\left(1 + \delta \sin\left(\frac{2\pi t}{365} + \theta\right)\right) \qquad \forall \ell \tag{3}$$

In our multistrain simulations, for purposes of illustration, we set both the shedding parameter ζ in Eq. 2 above and μ in Eq. A.16 to be 0.001. Obviously, it would be of considerable interest to know how the values of these two parameters impact strain proliferation, but this is left to future studies when data are available to guide simulations of realistic scenarios.

Acknowledgements and Funding Sources

This work was funded in part by NSF Grant 2032264 (PI: WMG).

medRxiv preprint doi: https://doi.org/10.1101/2021.06.07.21258504; this version posted June 11, 2021. The copyright holder for this preprint (which was not certified by peer review) is the author/funder, who has granted medRxiv a license to display the preprint in perpetuity. All rights reserved. No reuse allowed without permission.

References

[1] Anderson RM. The impact of vaccination on the epidemiology of infectious diseases. In: The Vaccine Book. Elsevier; 2016. p. 3–31.

[2] Kohli M, Maschio M, Becker D, Weinstein MC. The potential public health and economic value of a hypothetical COVID-19 vaccine in the United States: Use of cost-effectiveness modeling to inform vaccination prioritization. Vaccine. 2021;39(7):1157–1164.

[3] Eguia RT, Crawford KH, Stevens-Ayers T, Kelnhofer-Millevolte L, Greninger AL, Englund JA, et al. A human coronavirus evolves antigenically to escape antibody immunity. PLoS pathogens. 2021;17(4):e1009453.

[4] Jeyanathan M, Afkhami S, Smaill F, Miller MS, Lichty BD, Xing Z. Immunological considerations for COVID-19 vaccine strategies. Nature Reviews Immunology. 2020;20(10):615–632.

[5] Koopman JS, Simon CP, Getz WM, Salter R. Modeling the population effects of epitope specific escape mutations in SARS-CoV-2 to guide vaccination strategies. medRxiv. 2021;.

[6] Sariol A, Perlman S. Lessons for COVID-19 immunity from other coronavirus infections. Immunity. 2020;.

[7] Tai W, Wang Y, Fett CA, Zhao G, Li F, Perlman S, et al. Recombinant receptor-binding domains of multiple Middle East respiratory syndrome coronaviruses (MERS-CoVs) induce cross-neutralizing antibodies against divergent human and camel MERS-CoVs and antibody escape mutants. Journal of virology. 2017;91(1).

[8] Harvey WT, Carabelli AM, Jackson B, Gupta RK, Thomson EC, Harrison EM, et al. SARS-CoV-2 variants, spike mutations and immune escape. Nature Reviews Microbiology. 2021;p. 1–16.

[9] Saad-Roy CM, Levin SA, Metcalf CJE, Grenfell BT. Trajectory of individual immunity and vaccination required for SARS-CoV-2 community immunity: A conceptual investigation. Journal of the Royal Society Interface. 2021;18(175):20200683.

[10] Saad-Roy CM, Wagner CE, Baker RE, Morris SE, Farrar J, Graham AL, et al. Immune life history, vaccination, and the dynamics of SARS-CoV-2 over the next 5 years. Science. 2020;370(6518):811–818.

[11] Willem L, Verelst F, Bilcke J, Hens N, Beutels P. Lessons from a decade of individual-based models for infectious disease transmission: a systematic review (2006-2015). BMC infectious diseases. 2017;17(1):612.

[12] Chowell G, Sattenspiel L, Bansal S, Viboud C. Mathematical models to characterize early epidemic growth: A review. Physics of life reviews. 2016;18:66–97.

medRxiv preprint doi: https://doi.org/10.1101/2021.06.07.21258504; this version posted June 11, 2021. The copyright holder for this preprint (which was not certified by peer review) is the author/funder, who has granted medRxiv a license to display the preprint in perpetuity. All rights reserved. No reuse allowed without permission.

[13] Keskinocak P, Oruc BE, Baxter A, Asplund J, Serban N. The impact of social distancing on COVID19 spread: State of Georgia case study. Plos one. 2020;15(10):e0239798.

[14] Abueg M, Hinch R, Wu N, Liu L, Probert W, Wu A, et al. Modeling the effect of exposure notification and non-pharmaceutical interventions on COVID-19 transmission in Washington state. NPJ digital medicine. 2021;4(1):1–10.

[15] Chen PZ, Bobrovitz N, Premji Z, Koopmans M, Fisman DN, Gu FX. Heterogeneity in transmissibility and shedding SARS-CoV-2 via droplets and aerosols. eLife. 2021 apr;10:e65774. Available from: https://doi.org/10.7554/eLife.65774.

[16] van Doremalen N, Bushmaker T, Morris DH, Holbrook MG, Gamble A, Williamson BN, et al. Aerosol and Surface Stability of SARS-CoV-2 as Compared with SARS-CoV-1. New England Journal of Medicine. 2020;382(16):1564–1567. Available from: https://doi.org/10.1056/NEJMc2004973.

[17] Maginnis MS. Virus–receptor interactions: the key to cellular invasion. Journal of molecular biology. 2018;430(17):2590–2611.

[18] Challen R, Brooks-Pollock E, Read JM, Dyson L, Tsaneva-Atanasova K, Danon L. Risk of mortality in patients infected with SARS-CoV-2 variant of concern 202012/1: matched cohort study. bmj. 2021;372.

[19] Lavine JS, Bjornstad ON, Antia R. Immunological characteristics govern the transition of COVID-19 to endemicity. Science. 2021;371(6530):741–745.

[20] Alizon S, Luciani F, Regoes RR. Epidemiological and clinical consequences of within-host evolution. Trends in microbiology. 2011;19(1):24–32.

[21] Fenichel EP, Castillo-Chavez C, Ceddia MG, Chowell G, Parra PAG, Hickling GJ, et al. Adaptive human behavior in epidemiological models. Proceedings of the National Academy of Sciences. 2011;108(15):6306–6311.

[22] Gozzi N, Bajardi P, Perra N. The importance of non-pharmaceutical interventions during the COVID-19 vaccine rollout. medRxiv. 2021;Available from: https://www.medrxiv.org/content/early/2021/01/09/2021.01.09.21249480.

[23] Kumar A, Dowling WE, Román RG, Chaudhari A, Gurry C, Le TT, et al. Status Report on COVID-19 Vaccines Development. Current Infectious Disease Reports. 2021;23(6):1–12.

[24] Chretien JP, George D, Shaman J, Chitale RA, McKenzie FE. Influenza forecasting in human populations: a scoping review. PloS one. 2014;9(4):e94130.

medRxiv preprint doi: https://doi.org/10.1101/2021.06.07.21258504; this version posted June 11, 2021. The copyright holder for this preprint (which was not certified by peer review) is the author/funder, who has granted medRxiv a license to display the preprint in perpetuity. All rights reserved. No reuse allowed without permission.

[25] Getz WM, Gonzalez JP, Salter R, Bangura J, Carlson C, Coomber M, et al. Tactics and strategies for managing Ebola outbreaks and the salience of immunization. Computational and mathematical methods in medicine. 2015;2015.

[26] Getz WM, Salter R, Mgbara W. Adequacy of SEIR models when epidemics have spatial structure: Ebola in Sierra Leone. Philosophical Transactions of the Royal Society B. 2019;374(1775):20180282.

[27] Drake JM. Limits to forecasting precision for outbreaks of directly transmitted diseases. PLoS Med. 2005;3(1):e3.

[28] Jefferies JM, Clarke SC, Webb JS, Kraaijeveld AR. Risk of red queen dynamics in pneumococcal vaccine strategy. Trends in microbiology. 2011;19(8):377–381.

[29] Thomas LJ, Huang P, Yin F, Luo XI, Almquist ZW, Hipp JR, et al. Spatial heterogeneity can lead to substantial local variations in COVID-19 timing and severity. Proceedings of the National Academy of Sciences. 2020;117(39):24180–24187.

[30] Getz WM, Salter R, Luisa Vissat L, Horvitz N. A versatile web app for identifying the drivers of COVID-19 epidemics. Journal of Translational Medicine. 2021;19(1):1–20.

[31] Da Silva RM, Mendes CF, Manchein C. Scrutinizing the heterogeneous spreading of COVID-19 outbreak in large territorial countries. Physical Biology. 2021;18(2):025002.

[32] Zhang J, Litvinova M, Liang Y, Wang Y, Wang W, Zhao S, et al. Changes in contact patterns shape the dynamics of the COVID-19 outbreak in China. Science. 2020;.

[33] Udwadia ZF, Raju RS. How to protect the protectors: 10 lessons to learn for doctors fighting the COVID-19 coronavirus. Medical Journal, Armed Forces India. 2020;.

[34] Van Damme W, Dahake R, van de Pas R, Vanham G, Assefa Y. COVID-19: Does the infectious inoculum dose-response relationship contribute to understanding heterogeneity in disease severity and transmission dynamics? Medical hypotheses. 2021;146:110431.

[35] Zhao Z, Li H, Wu X, Zhong Y, Zhang K, Zhang YP, et al. Moderate mutation rate in the SARS coronavirus genome and its implications. BMC evolutionary biology. 2004;4(1):1–9.

[36] Geoghegan JL, Holmes EC. The phylogenomics of evolving virus virulence. Nature Reviews Genetics. 2018;19(12):756–769.

[37] Larsen LG, Eppinga MB, Passalacqua P, Getz WM, Rose KA, Liang M. Appropriate complexity landscape modeling. Earth-science reviews. 2016;160:111–130.

medRxiv preprint doi: https://doi.org/10.1101/2021.06.07.21258504; this version posted June 11, 2021. The copyright holder for this preprint (which was not certified by peer review) is the author/funder, who has granted medRxiv a license to display the preprint in perpetuity. All rights reserved. No reuse allowed without permission.

[38] Yang P, Yang G, Qi J, Sheng B, Yang Y, Zhang S, et al. The effect of multiple interventions to balance healthcare demand for controlling COVID-19 outbreaks: a modelling study. Scientific reports. 2021;11(1):1–13.

[39] Baker RE, Park SW, Yang W, Vecchi GA, Metcalf CJE, Grenfell BT. The impact of COVID-19 nonpharmaceutical interventions on the future dynamics of endemic infections. Proceedings of the National Academy of Sciences. 2020;117(48):30547–30553.

[40] Greaney AJ, Starr TN, Gilchuk P, Zost SJ, Binshtein E, Loes AN, et al. Complete mapping of mutations to the SARS-CoV-2 spike receptor-binding domain that escape antibody recognition. Cell host & microbe. 2021;29(1):44–57.

[41] Brüssow H. COVID-19: emergence and mutational diversification of SARS-CoV-2. Microbial Biotechnology. 2021;14(3):756–768.

[42] Keeling MJ, Eames KT. Networks and epidemic models. Journal of the Royal Society Interface. 2005;2(4):295–307.

[43] Roberts GO, Rosenthal JS, et al. General state space Markov chains and MCMC algorithms. Probability Surveys. 2004;1:20–71.

[44] Lele SR, Dennis B, Lutscher F. Data cloning: easy maximum likelihood estimation for complex ecological models using Bayesian Markov chain Monte Carlo methods. Ecology letters. 2007;10(7):551–563.

[45] Suthar MS, Zimmerman MG, Kauffman RC, Mantus G, Linderman SL, Hudson WH, et al. Rapid generation of neutralizing antibody responses in COVID-19 patients. Cell Reports Medicine. 2020;1(3):100040.

[46] Muruato AE, Fontes-Garfias CR, Ren P, Garcia-Blanco MA, Menachery VD, Xie X, et al. A high-throughput neutralizing antibody assay for COVID-19 diagnosis and vaccine evaluation. Nature communications. 2020;11(1):1–6.

[47] Tkachenko AV, Maslov S, Elbanna A, Wong GN, Weiner ZJ, Goldenfeld N. Time-dependent heterogeneity leads to transient suppression of the COVID-19 epidemic, not herd immunity. Proceedings of the National Academy of Sciences. 2021;118(17).

[48] Koyama T, Weeraratne D, Snowdon JL, Parida L. Emergence of drift variants that may affect COVID-19 vaccine development and antibody treatment. Pathogens. 2020;9(5):324.

[49] Getz WM, Lloyd-Smith JO. Basic methods for modeling the invasion and spread of contagious diseases. DIMACS Series in Discrete Mathematics and Theoretical Computer Science. 2006;71:87.

[50] McCallum H, Barlow N, Hone J. How should pathogen transmission be modelled? Trends in ecology & evolution. 2001;16(6):295–300.

medRxiv preprint doi: https://doi.org/10.1101/2021.06.07.21258504; this version posted June 11, 2021. The copyright holder for this preprint (which was not certified by peer review) is the author/funder, who has granted medRxiv a license to display the preprint in perpetuity. All rights reserved. No reuse allowed without permission.

[51] Anderson RM, May RM, et al. Coevolution of hosts and parasites. Parasitology. 1982;85(Pt 2):411–426.

[52] Getz WM, Salter R, Lyons AJ, Sippl-Swezey N. Panmictic and clonal evolution on a single patchy resource produces polymorphic foraging guilds. PloS one. 2015;10(8):e0133732.

[53] Hussein M, Toraih E, Elshazli R, Fawzy M, Houghton A, Tatum D, et al. Meta-analysis on serial intervals and reproductive rates for SARS-CoV-2. Annals of surgery. 2021;273(3):416–423.

[54] Grimm V, Mengel F, Schmidt M. Extensions of the SEIR model for the analysis of tailored social distancing and tracing approaches to cope with COVID-19. Scientific Reports. 2021;11(1):1–16.

[55] Wu SL, Mertens AN, Crider YS, Nguyen A, Pokpongkiat NN, Djajadi S, et al. Substantial underestimation of SARS-CoV-2 infection in the United States. Nature communications. 2020;11(1):1–10.

[56] Munnink BBO, Nieuwenhuijse DF, Stein M, O'Toole Á, Haverkate M, Mollers M, et al. Rapid SARS-CoV-2 whole-genome sequencing and analysis for informed public health decision-making in the Netherlands. Nature medicine. 2020;26(9):1405–1410.

[57] Kramer A, Schwebke I, Kampf G. How long do nosocomial pathogens persist on inanimate surfaces? A systematic review. BMC infectious diseases. 2006;6(1):1–8.

[58] Liu X, Huang J, Li C, Zhao Y, Wang D, Huang Z, et al. The role of seasonality in the spread of COVID-19 pandemic. Environmental research. 2021;195:110874.

[59] Valtonen A, Molleman F, Chapman CA, Carey JR, Ayres MP, Roininen H. Tropical phenology: Bi-annual rhythms and interannual variation in an Afrotropical butterfly assemblage. Ecosphere. 2013;4(3):1–28.

[60] Getz WM, Salter R, Muellerklein O, Yoon HS, Tallam K. Modeling epidemics: A primer and Numerus Model Builder implementation. Epidemics. 2018;25:9–19.

[61] Lythgoe KA, Hall M, Ferretti L, de Cesare M, MacIntyre-Cockett G, Trebes A, et al. SARS-CoV-2 within-host diversity and transmission. Science. 2021;372(6539). Available from: https://science.sciencemag.org/content/372/6539/eabg0821.

[62] Jones JH. Notes on R0. Califonia: Department of Anthropological Sciences. 2007;323.

medRxiv preprint doi: https://doi.org/10.1101/2021.06.07.21258504; this version posted June 11, 2021. The copyright holder for this preprint (which was not certified by peer review) is the author/funder, who has granted medRxiv a license to display the preprint in perpetuity. All rights reserved. No reuse allowed without permission.

Figures and Tables

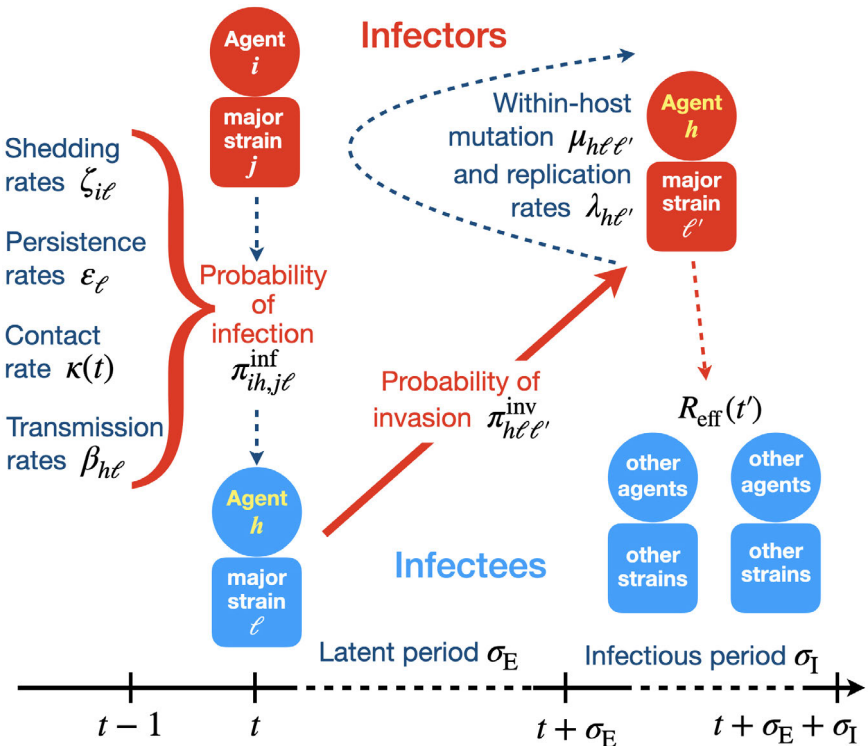

Figure 1: An overview of the processes included in our SEIVD-IBM model. The probability $\pi^{\text{inf}}_{ih,jl}$ of A_h being infected primarily with pathogen ℓ in terms of receiving an effective dose from agent A_i, (η) is computed in terms of a concatenation of shedding rates $(\zeta_{i\ell})$, environmental persistence rates (ε_ℓ), and host transmission $(\beta_{h\ell})$ processes (Eq. A.15) and includes both waning and cross immunity factors. The probability $\pi^{\text{inv}}_{h\ell\ell'}$ that the dominant strain emerging in host A_h is strain ℓ' given initial infection with strain ℓ is computed in terms of within-host mutation and within-host replication process (Eq. A.16) and also includes both waning and cross immunity factors. These two probabilities are then used to compute the overall probability $\pi_{ih,j\ell'}$ (Eq. A.17) that infector i, infected with major strain j, infects infectee h with major strain ℓ'. The quantity $R_{\text{eff}}(t')$ is the expected number of individuals each infectious agent is expected to infect around time $t' \in [t+\sigma_{\text{E}}, t+\sigma_{\text{E}}+\sigma_{\text{I}}]$, where $R_0 = R_{\text{eff}}(0)$ is estimated for our model using Eq. A.29. Equation references for the other mathematical functions provided in this figure are given in Table 2.

medRxiv preprint doi: https://doi.org/10.1101/2021.06.07.21258504; this version posted June 11, 2021. The copyright holder for this preprint (which was not certified by peer review) is the author/funder, who has granted medRxiv a license to display the preprint in perpetuity. All rights reserved. No reuse allowed without permission.

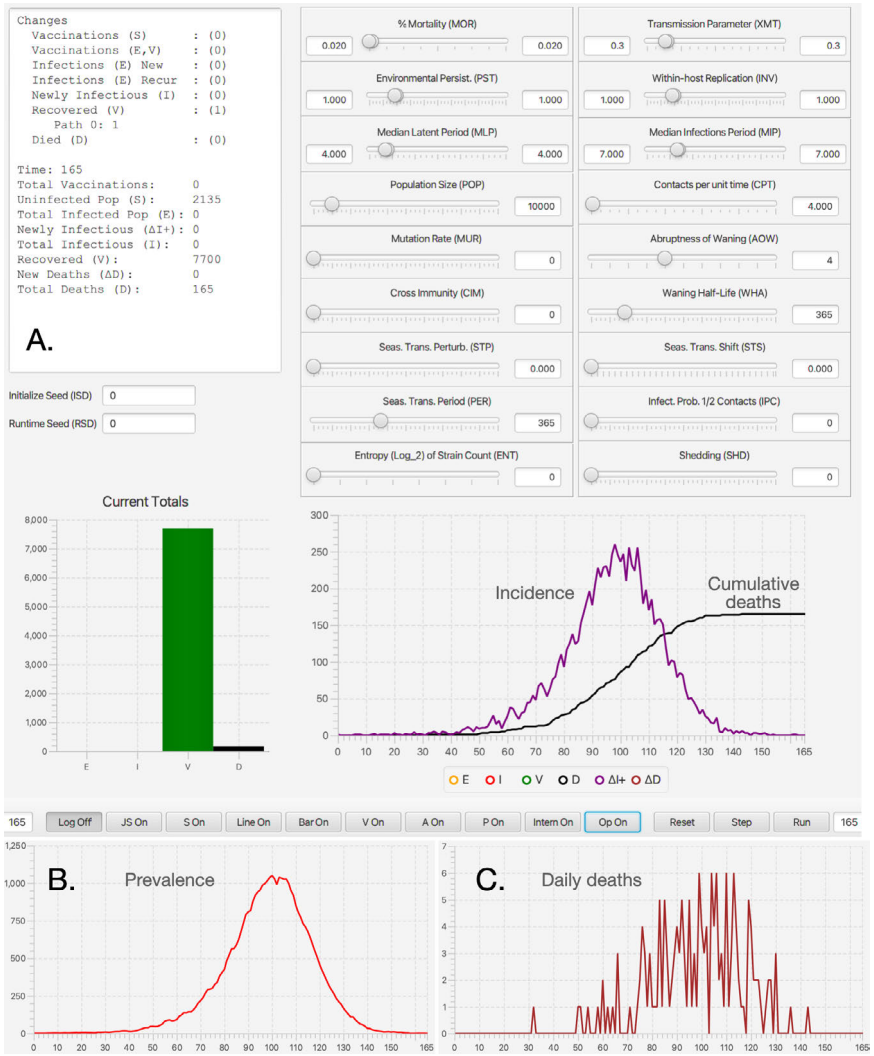

Figure 2: **A.** The dashboard of our Java Runtime-Alterable-Model Platform (J-RAMP) SEIVD (S=susceptibles, E=exposed, I=infectious, V=immune, D=dead) individual-based model (IBM) and simulations obtained using the parameters values depicted in the slider windows (also see Table 1). The top left window of this dashboard contains information on the final state of the population (in this case $S = 2135$ and $D = 165$ in a population of $N_0 = 10,000$), the bottom left bar graph of dashboard panel is the final values of E, I, V and D at epidemic cessation at time $t = 166$ (days) or the simulation run time, whichever comes first. Dashboard also shows a graph of incidence and cumulative deaths (purple and black: selected using colored buttons below the graph). The bottom ribbon of the dash board has a series of radio buttons that respectively open a Log, a JavaScript (JS), and a Scripting (S) window, Line and Bar graph windows (for multistrain runs), as well as windows for controlling vaccination strategies (V), listing realtime agent information (A), pathogen parameter values (P), monitoring probability computations (Intern), coding and controlling runtime alternative operations (Op), and three runtime buttons (Reset, Step, Run). **B.** Graphs of prevalence (cut out from main panel when only the red button is on) and **C.** daily deaths (crimson button) are pasted below the dashboard.

medRxiv preprint doi: https://doi.org/10.1101/2021.06.07.21258504; this version posted June 11, 2021. The copyright holder for this preprint (which was not certified by peer review) is the author/funder, who has granted medRxiv a license to display the preprint in perpetuity. All rights reserved. No reuse allowed without permission.

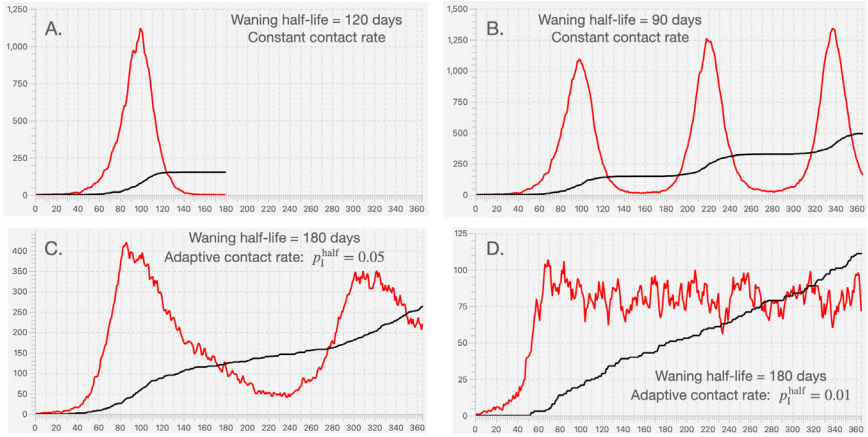

Figure 3: Plots of prevalence (I: red) and dead (D: black) individuals for simulations using the parameter values given in Table 1 with $N = 10,000$. The waning immunity half-life values are $t^{\text{half}} = 90$, 120 or 180, as labeled. In the top two panels the contact rate is constant, while in the bottom two panels it is adaptive with $p_{\text{I}}^{\text{half}} = 0.05$ or 0.01 as labeled (Eq. A.10). Note that the adaptive case approaches the constant case as $p_{\text{I}}^{\text{half}} \to \infty$ and that the vertical axis in the four panels each have different scale, though the horizontal time axes is the same in all four case (365 days).

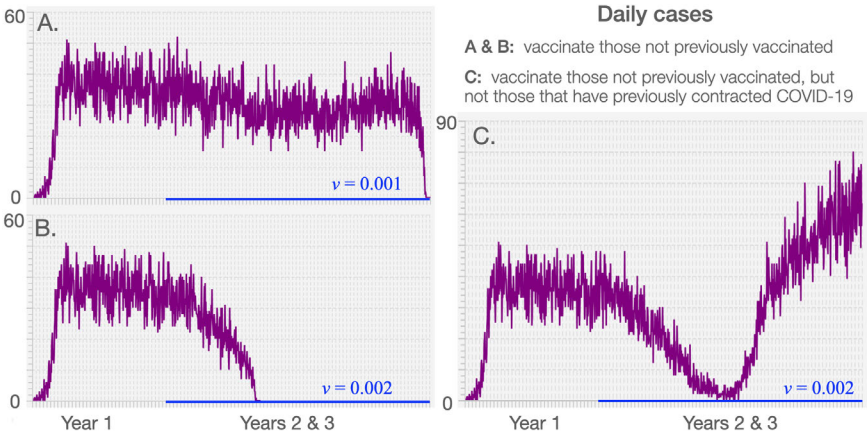

Figure 4: Incidence (ΔI^+: purple) is plotted over 3 years for the baseline run (parameters given in Table 1 with $N = 100,000$, $p_{\text{I}}^{\text{half}} = 0.002$, and $t_v^{\text{half}} = 365$) for the cases where vaccination rates $v(t)$ (indicated by blue lines) are applied during the second and third years only to individuals not previously vaccinated selected at random (**A**. $v(t) = 0.001$, **B**. $v(t) = 0.002$) and to individuals not previously vaccinated and who also have not previously been infected with SARS-CoV-2 (**C**. $v(t) = 0.002$).

medRxiv preprint doi: https://doi.org/10.1101/2021.06.07.21258504; this version posted June 11, 2021. The copyright holder for this preprint (which was not certified by peer review) is the author/funder, who has granted medRxiv a license to display the preprint in perpetuity. All rights reserved. No reuse allowed without permission.

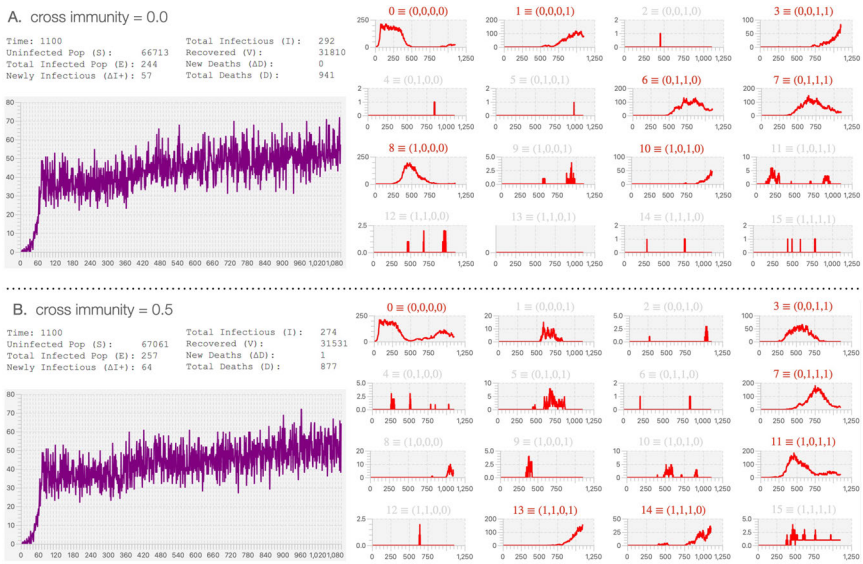

Figure 5: The total daily incidence (ΔI+: purple) and strain-specific prevalence (I: red) individuals for a 16-strain epidemic burning through a population of size $N = 100,000$ are plotted over a 3-year period for the cases where cross-immunity is absent (A. $c = 0.0$) or intermediate among nearest neighbors differing by one allele (B. $c = 0.5$). The remaining parameters are listed in Table 1 and for all strains include the same host transmission ($\bar{\beta} = 0.3$) and virulence ($p_\alpha = 0.02$), waning half-life $t^{\text{half}} = 365$, minor strain shedding $\zeta = 0.001$ and within host mutation ($\mu = 0.001$) parameter values. Note that each panel has its own vertical scale and that the horizontal scales are set by the J-RAMP and are 0-1100 days for the incidence curves and 0-1250 days for the prevalence curves, although all curves are drawn to 1100 days. Dominant or codominant strains are labeled in red (number and equivalane allele representation), while minor strains are labeled in light grey.

medRxiv preprint doi: https://doi.org/10.1101/2021.06.07.21258504; this version posted June 11, 2021. The copyright holder for this preprint (which was not certified by peer review) is the author/funder, who has granted medRxiv a license to display the preprint in perpetuity. All rights reserved. No reuse allowed without permission.

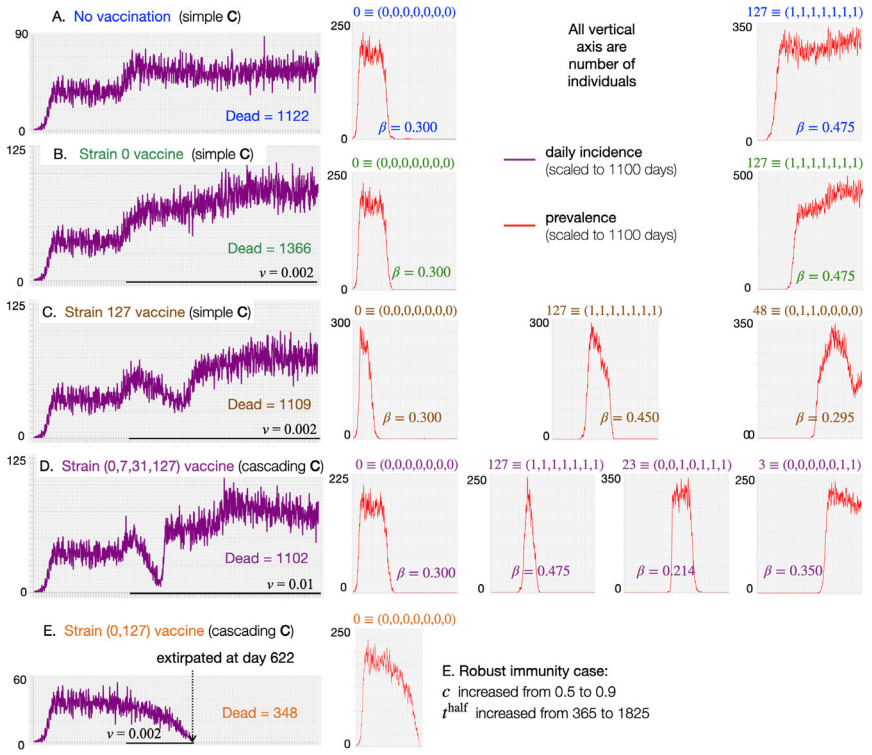

Figure 6: Daily incidence (deep purple curves) and prevalence of individual strains (red curves; with strain number labels plotted in order of emergence over time) that exceed a maximum prevalence of 12 individuals at any time are plotted over a three year period ($t \in [0, 1100]$ days), firstly, for three cases (**A.**-**C.** in a system with nearest-neighbor only cross-immunity (labeled "simple", see Eq. 1) and, secondly, in two cases (**D.** and **F.**) in a system with cascading cross-immunity (Eq. A.7). In the first three cases we have: **A.**, no vaccination (blue labels); an **B.** & **C.**, a vaccination rate of $v = 0.002$ applied in years 2 and 3 ($t \in [365, 110]$) to individuals who have not previously been vaccinated, respectively for the cases of univalent vaccines (strain 0, green labels and strain 127, brown labels). In the fourth case, **D.**, a quadravalent vaccine (strain 0, 7, 31 & 127; plum labels) is applied at a vaccination rate of $v = 0.01$ (i.e., 1%) at random, irrespective whether or not individuals selected have been previously vaccinated (or ill with COVID-19). In the fifth case, **E** ("robust immunity case"), a bivalent vaccine (strains 0 & 127; orange labels) is applied, as in cases **B.** & **C.**, at a vaccination rate of $v = 0.002$ (i.e., 1%) at random to individuals selected that have been previously vaccinated. In this latter case, however immune waning has been reduced by a factor of 5 ($t^{\text{half}} = 1825$ days) with cascading cross immunity increased from $c = 0.5$ to $c = 0.9$. The dashboards for all these cases, and miniature prevalence plots of all 128 strains for each of these four cases can be found in Figs. C.5-C.9 in the Appendix. The parameter values are the same as in Fig. 5B, apart from the immune parameters being greatly strengthen in the "robust immunity case" **E.**, and in all cases strain specific transmission parameter values β_j ($j = 0, ..., 127$) that were randomly assigned values between 0 and 0.3, except for the increasingly dominant strain sequence $\beta_0 = 0.3$ ($0 \equiv (0, 0, 0, 0, 0, 0, 0)$), $\beta_1 = 0.325$ ($1 \equiv (0, 0, 0, 0, 0, 0, 1)$), $\beta_3 = 0.35$ ($\equiv (0, 0, 0, 0, 0, 1, 1)$),..., $\beta_{127} = 0.475$ ($127 \equiv (1, 1, 1, 1, 1, 1, 1)$) (particular values of β_j are provided for the different strains depicted here; see Table in Fig. C.4 for all values of β_j, $j = 0, ..., 127$). Note that the vertical axis are all on the same scale height for incidence, but are individually scaled for prevalence, while the time axis are all on the same scale for the prevalence curves which differs from the incidence curves, which among themselves are all on the same time scale.

medRxiv preprint doi: https://doi.org/10.1101/2021.06.07.21258504; this version posted June 11, 2021. The copyright holder for this preprint (which was not certified by peer review) is the author/funder, who has granted medRxiv a license to display the preprint in perpetuity. All rights reserved. No reuse allowed without permission.

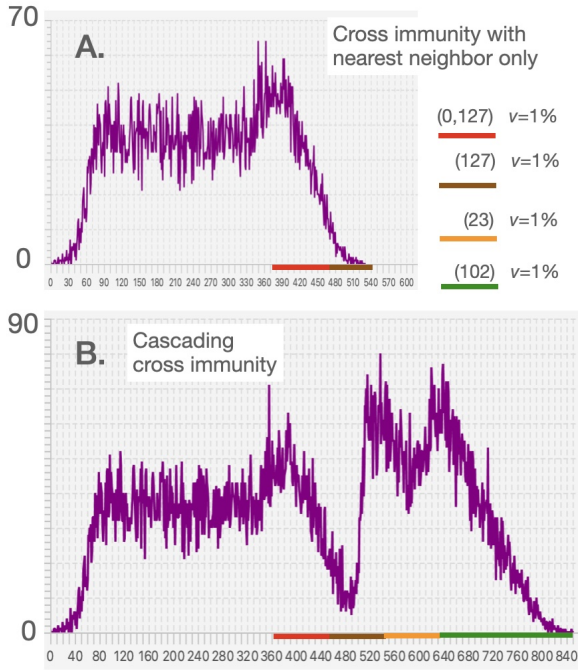

Figure 7: The daily incidences (vertical axis: number of individuals) are plotted over time (horizontal axis: number of days; plots have been squashed to ensure they are all on the same time scale) for two cases: **A.** adaptive vaccination for nearest-neighbor only cross immunity (Eq. 1) and **B.** adaptive vaccination for cascading cross immunity case (Eq. A.7), and should be compared with the non-vaccination case depicted in Fig. 6A and the non-adaptive vaccination case depicted in Fig. 6D. As in this latter non-adaptive case, vaccination is performed on non-infectious individuals, selected at random (i.e., re-vaccinations can occur) at a rate of 1% per day, but now the dominant strain is targeted, as well as a second strain if its prevalence exceeds 10 cases, with vaccine valency switches every 90 days. The realized adaptive vaccine valencies for these two runs are indicated by colored bars on the horizontal time axis (red, valency is (0,127); brown, valency is (127); orange, valency is (23); green, valency is (102)).

medRxiv preprint doi: https://doi.org/10.1101/2021.06.07.21258504; this version posted June 11, 2021. The copyright holder for this preprint (which was not certified by peer review) is the author/funder, who has granted medRxiv a license to display the preprint in perpetuity. All rights reserved. No reuse allowed without permission.

Table 1: Parameter values used to simulate single and multistrain outbreaks

Parameter	Symbol	Value	Source/Comment
Single strain simulations			
Time unit	t	daily	Goldilocks value*
Nominal pop size	N_0	1 to 10 $\times 10^4$	Goldilocks value‡
Basic contact rate	κ_0	4 per day	effective contacts†
Transmission	β	0.3	ensures $R_0 \approx 3^+$
Latent Period	σ_{E}	4 days	median time in E¶
Infectious period	σ_{I}	7 days	median time in I§
Immunity half-life	t^{half}	1/4 to 1 year	per run specs.‖
Disease-induced mort.**	p_α	2% of cases	mortality rate is $\alpha^{\#}$
Adaptive contact param.*†	$p_{\mathrm{I}}^{\mathrm{half}}$	0, 0.002, 0.05	reduces κ from κ_0
Seasonal fluctuation param.	δ	0	seasons ignored*+
Multi strain simulations (single strain parameter values for all strains if not mentioned below)			
Mutation rate*‡	μ	0.001*#	See Eq. A.16
Strain number	$j = 0, ..., 2^J - 1$	J is 1 to 8	i.e., 2 to 1024 strains
Cross immunity	c_{jm}	0 & 0.5	See Eq. 1
Pathogen shedding	$\bar{\zeta}_{jm}$	0.001*#	See Eq. A.12
Environmental persistence	$\bar{\eta}_j$	1 for all j	See Eq. A.13
Transmission	$\bar{\beta}_j$	[0,0.475]	per run specs.
Within-host replication rate	λ_j	1 for all j	See Eq. A.16
Disease-induced mort.**	p_{α_j}	[0,0.05]	per run specs.

*Weekly unit produced excessive variation (see SOI)

‡Trade-off between excessive demographic stochasticity and simulation run time

†Sufficiently long and close to make transmission possible (also see Eq. A.29)

+See Eq. A.29

¶Reciprocal of γ in continuous time computation of R_0 per Eq. A.29

§Reciprocal of ρ in continuous time computation of R_0 per Eq. A.29

‖See Eq. A.6: note $w(t)$ switches from 1 to 0 as immunity goes from complete to absent

#This is "virulence" parameter of continuous-time SEIR models

**If $\alpha << 1$ then $p_{\alpha_j} = 1 - e^{-\alpha} \approx \alpha$

*†See Eq. A.10. Mostly 0.002 is used. Setting $p_{\mathrm{I}}^{\mathrm{half}} = 0$ implements $\kappa(t) = \kappa_0$, though $\kappa(t) \to \kappa_0$ as $p_{\mathrm{I}}^{\mathrm{half}} \to \infty$

*+Implies values of k and θ in Eq. A.13 are irrelevant

*‡Strain independent—strain dependence requires more elaborate model

*#Quantifies the pass-on rate of mutations rather than the mutational rate of a locus or gene

***If $\alpha_j << 1$ then $p_{\alpha_j} = 1 - e^{-\alpha_j} \approx \alpha_j$

medRxiv preprint doi: https://doi.org/10.1101/2021.06.07.21258504; this version posted June 11, 2021. The copyright holder for this preprint (which was not certified by peer review) is the author/funder, who has granted medRxiv a license to display the preprint in perpetuity. All rights reserved. No reuse allowed without permission.

Table 2: Variables, indices and functions used in the model

Symbols	Variables and indices	Equation
Variables		
$N_{\mathrm{S}}(t)$, $N_{\mathrm{A}}(t)$, $N_{\mathrm{D}}(t)$	size of sets **S**, **A** and **D**	Eq. A.1
J, j, m, ℓ and ℓ'	strain entropy and indices $(0, ..., 2^J - 1)$	Eq. A.2
$N_{\mathrm{I}}(t)$, $N_{\mathrm{I}_j}(t)$	number of infectious: total and strain j at time t	
A_i, A_h	specific agents $i, h = 1, ..., N_{\mathrm{A}}(t)$ in set **A**	Eq. A.4
Functions		
$\omega_{ij}(t)$	waning immunity of A_i w.r.t. strain j	Eq. A.6
$\kappa(t)$	adaptive contact rate	Eq. A.10
$\phi_{ij}(t)$	immunity modifier	Eq. A.11
$\zeta_{ij}(t)$	shedding rate of strain j by infector A_i	Eq. A.12
$\eta_\ell(t)$	environmental persistence	Eq. A.13
$\beta_{h\ell}(t)$	strain transmission to infectee A_h	Eq. A.14
$\pi^{\mathrm{inf}}_{ih,j\ell}(t)$	probability A_i infects A_h	Eq. A.15
$\pi^{\mathrm{inv}}_{h\ell\ell'}(t)$	probability ℓ' is major strain when ℓ invades	Eq. A.16
$\pi_{ih,j\ell'}(t)$	probability ℓ' is major strain in A_h when j is major strain in A_i	Eq. A.17

medRxiv preprint doi: https://doi.org/10.1101/2021.06.07.21258504; this version posted June 11, 2021. The copyright holder for this preprint (which was not certified by peer review) is the author/funder, who has granted medRxiv a license to display the preprint in perpetuity. All rights reserved. No reuse allowed without permission.

APPENDICES

A Model Construction

Here we formulate an individual-based or agent-based (ABM) SEIR epidemiological model to include host immunological waning and pathogen genetic drift with variation across strain transmissibility and virulence. [1]

Assumptions, definitions, and states

The population consists of a well-mixed pool of N_0 individuals that is homogeneous except for the fact that some are uninfected (denoted S), some currently infected (E: exposed and not yet infectious; I infectious and asymptomatic or symptomatic) or have been infected and are now either dead (D) or recovered/vaccinated with some level of immunity (V) to one or more of 2^J pathogen strains. This immunity wanes over time and its current level, augmented by specified levels of strain cross-immunity, factored into an agent specific time-dependent strain-resistance function that impacts the shedding of mutant strains by infectors and the within-host replication rates of mutant strains in infectees.

At the start of the epidemic, all individuals are assumed to encounter, on average, $\kappa_0 > 0$ other individuals during each time period $[t, t+1]$, but this "effective contacts" rate adaptively decreases with increasing prevalence of the disease due to the implementation of non-pharmaceutical interventions (social distancing, hand washing, mask wearing, and other hygienic precautions). In our selection of epidemiological parameter values, a unit of time is taken to be a 24-hour day. Other scalings of time would then require appropriately adjusted epidemiological parameter values. Refined versions of the model could include age-related parameter values and contact rates, as well as contact tracing, quarantining, and isolation of infected individuals; but these will not be considered here.

Initially, at model time $t = 0$, all individuals are considered SARS-CoV-2 naïve susceptible apart from one individual who is considered to have just entered the infectious stage, infected by a pathogen designated as pathogen strain 0 (wildtype). Throughout the model simulation, the N_0 agents in the population are partitioned into three disjoint sets: the set of SARS-CoV-2 naïve individuals, $\mathbf{S}(t)$, containing $N_{\mathrm{S}}(t)$ (the susceptibles); the set of identified agents, $\mathbf{A}(t)$, containing $N_{\mathrm{A}}(t)$ individuals who are either currently infected (time t) with a particular strain of SARS-CoV-2, or have some level of waning immunity to one or more strains of SARS-CoV-2; and the set of dead individuals $\mathbf{D}(t)$, currently of size $N_{\mathrm{D}}(t)$. Only the individuals in $\mathbf{A}(t)$ are uniquely identified as they become infected for the first time and make the transition from set $\mathbf{S}(t)$ to set $\mathbf{A}(t)$, where they are sequentially labeled using the index $i = 1, ..., N_{\mathrm{A}}(t)$. The single infected individual at time zero will be designated Agent 1 (also known as patient zero and denoted by A_1). Thus at time t it follows that

$$N_{\mathrm{S}}(t) + N_{\mathrm{A}}(t) + N_{\mathrm{D}}(t) = N_0 \quad \text{(a constant)} \tag{A.1}$$

We note that individuals in set $\mathbf{A}(t)$ can be in a disease state E or I with respect to pathogen j, but simultaneously can be in multiple immune states if

medRxiv preprint doi: https://doi.org/10.1101/2021.06.07.21258504; this version posted June 11, 2021. The copyright holder for this preprint (which was not certified by peer review) is the author/funder, who has granted medRxiv a license to display the preprint in perpetuity. All rights reserved. No reuse allowed without permission.

they have been infected with more than one pathogen strain in the past. We also note that the distinction between symptomatic and asymptomatic individuals in state I will not be considered here; and only need be incorporated if testing, quarantining, and treatment processes are included in the model.

The total number of pathogen strains is set by a parameter $J > 0$, where each pathogen is represented by a J-bit binary number. Thus, there are 2^J possible strains indexed by $j = 0, 1, 2, \ldots, 2^J - 1$ where j is the decimal equivalent that corresponds to a given binary string. The initial strain, $j = 0$ is the binary string of J zeros.

Sets of stochastic epidemic events (i.e., transitions from classes S to E, E to I, I to V or D) are implemented at consecutive integer points in time (one set of events for each point in time). Events will only be considered on individuals that have been infected by at least one of the pathogens at some time after $t = 0$ (this means that initially the epidemic computation proceeds rather rapidly, but becomes more computationally intensive for each time step as time proceeds).

Pathogen set

At the start of the simulation ($t = 0$), the set of potential pathogens indexed by $j = 0, ..., 2^J - 1$ is generated along with its associated environmental persistence ($\bar{\eta}_j$), transmission ($\bar{\beta}_j$), within host replication (λ_j) and disease-induced mortality rate (probability of dying from the disease p_{α_j}) parameters. These may be specified or drawn from underlying distributions (e.g., the uniform distributions $\beta \sim \texttt{Uniform}[\beta_{\min}, \beta_{\max}]$ and so on). Also, our model includes two $2^J \times 2^J$ matrices of constants that are associated with pathogen mutations during strain shedding (elements ζ_{jm}) and cross-immunity (elements c_{jm}) processes and thus involve but are conditioned on either the major strain that an infector is harboring or on immunological state of the agents involved. These are the shedding and cross-immunity matrices with elements $j, m = 1, ..., 2^J - 1$, Thus we generate the following list of parameters associated with our 2^J pathogen strains:

$$\begin{aligned} \text{Pathogen list} \quad &= \\ &\left\{ \left(\bar{\eta}_j, \bar{\beta}_j, \lambda_j, p_{\alpha_j};\ \zeta_{jm} \text{ and } c_{jm} \text{ for } m = 0, ..., 2^J - 1\right) \,\middle|\, j = 0, ..., 2^J - 1 \right\} \end{aligned} \tag{A.2}$$

Agent states

In accordance with the above set of assumptions, each agent has the following basic disease states at time t, where disease states in agent A_i are referenced by the time $\tau_j > 0$ at which the most recent infection with strain j has occurred (an individual may be re-infected after immunity to the strain has waned to relatively low levels):

1. $\mathrm{S}(t)$: An individual who at time t has not been infected with any strain of the pathogen up to time t. All these individuals belong to set $\mathbf{S}(t)$

2. $\mathrm{E}_j(t, \tau_{ij})$: An agent A_i who was infected with strain j at time τ_{ij}, but has not yet become infectious (this is an individual in the latent stage that lasts for σ_{E} units of time). All these individuals belong to set $\mathbf{A}(t)$

medRxiv preprint doi: https://doi.org/10.1101/2021.06.07.21258504; this version posted June 11, 2021. The copyright holder for this preprint (which was not certified by peer review) is the author/funder, who has granted medRxiv a license to display the preprint in perpetuity. All rights reserved. No reuse allowed without permission.

3. $\mathrm{I}_j(t, \tau_{ij})$: An agent A_i who is currently infectious with strain j, after being infected with strain j at time τ_{ij} (this is the infectious stage that lasts for σ_{I} units of time). All these individuals belong to set $\mathbf{I}(t) \subseteq \mathbf{A}(t)$

4. $\mathrm{V}_j(t, \tau_{ij})$: An agent A_i who was infectious with strain j, having been infected with strain j at time τ_{ij}, but is now non-infectious with regard to this strain—that is, recovered with some immunity to strain j, as well as some cross immunity to strains closely related to j. All these individuals belong to set $\mathbf{A}(t)$

5. $\mathrm{D}(t)$: An individual at time t who has died after being exposed to and become infectious with some strain of the pathogen. In a refined version of the model, a record will be kept of the time of death and the strain that caused death. All these individuals belong to set $\mathbf{D}(t)$.

Since an agent A_i may be infected over time by more than one strain j, its complete epidemiological state is represented by a list

$$\mathrm{A}_i(t) = \{\text{state w.r.t. pathogen } 0, \cdots, \text{state w.r.t. pathogen } 2^J - 1\} \tag{A.3}$$

If a living agent does not fall into any of the categories $2 - 4$ with respect to pathogen j, we denote its epidemiological state at position j as $\emptyset$ (the empty set). Consequently, if an agent A is susceptible at time t (i.e., an element of $S(t)$), then we write

$$\mathrm{A}_0(t) = \{\emptyset, \ldots, \emptyset\} \in \mathbf{S}$$

However, while such individuals are omitted from the A list (hence we did not subscript the agent A above), they may be recognized as "virtual members" with this implicit state. Some other examples are:

- If $\mathrm{A}_i(t)$ is infected, but not yet infectious, with pathogen strain j at time t but has not been infected with any other pathogen in its past history, then
$$\mathrm{A}_i(t) = \{\emptyset, \cdots, \emptyset, \mathrm{E}_j(t, \tau_j), \emptyset, \cdots, \emptyset\}$$

- On the other hand if A_i recovered from an infection with pathogen 0 at time τ_0, and is now in infectious with pathogen j at time t, having become infected with this pathogen at time τ_j then we write
$$\mathrm{A}_i(t) = \{\mathrm{V}_0(t, \tau_0), \emptyset, \cdots, \emptyset, \mathrm{I}_j(t, \tau_j), \emptyset, \cdots, \emptyset\}$$

As we shall see, an agent history may contain at most one instance of either E_j or I_j, while possibly containing multiple instances of V_j.

Agent and index sets

At the start of each time period, we update the set of identified agents $\mathbf{A}$ by adding susceptibles that became infected with pathogens during the previous time period and removing agents that died during the previous time period. Thus if $\mathbb{I}_{\mathrm{A}}$ is the index set for non-empty elements of $\mathbf{A}$, with new indices added

medRxiv preprint doi: https://doi.org/10.1101/2021.06.07.21258504; this version posted June 11, 2021. The copyright holder for this preprint (which was not certified by peer review) is the author/funder, who has granted medRxiv a license to display the preprint in perpetuity. All rights reserved. No reuse allowed without permission.

for newly infected susceptibles and indices removed for individuals that died, then by definition:

$$\mathbf{A}(t+1) = \{\mathrm{A}_i(t+1) | i \in \mathbb{I}_\mathrm{A}(t+1)\} \tag{A.4}$$

where the number of indices in the updated set $\mathbb{I}_\mathrm{A}(t+1)$ is $N_\mathrm{A}(t+1)$ and the updated number of dead is $N_\mathrm{D}(t+1)$ at time $t+1$.

For mathematical convenience all susceptibles S will also be referred to as A_0:, i.e., there are $N_\mathrm{S}(t)$ individuals referenced by A_0 at time t. It will be useful to partition the set $\mathbf{A}(t)$ itself into three subsets at time t by identifying the sets $\mathbf{E}(t)$ and $\mathbf{I}(t)$ which respectively contain all agents that are currently in a state $\mathrm{E}_j(t)$ or a state $\mathrm{I}_j(t)$ at time t for some $j = 0, ..., 2^J - 1$. We note the intersection of these two sets is empty—i.e., $\mathbf{E}(t) \cap \mathbf{I}(t) = \emptyset$—as will become apparent below from the transmission process rules set up below. We will use the notation

$$\mathbf{A}_\mathrm{S}(t) = \mathbf{A}(t) \setminus \big(\mathbf{E}(t) \cup \mathbf{I}(t)\big) \tag{A.5}$$

to denote the set of agents in $\mathbf{A}(t)$ but not in $\mathbf{E}(t)$ or $\mathbf{I}(t)$.

We also identify the set of infectious agents with infectious strain j. If A^j denotes an agent whose epidemiological state contains an entry $\mathrm{I}_j(t, _)$, then

$$\mathbf{I}_j(t) = \{\mathrm{A}^j_{i_1}(t), \mathrm{A}^j_{i_2}(t), \ldots, \mathrm{A}^j_{i_{N_{\mathrm{I}_j}}}(t)\},$$

where the number of such agents is denoted by $N_{\mathrm{I}_j}(t)$, and its index set by

$$\mathbb{I}_{\mathrm{I}_j}(t) = \{i_{1_j}, \ldots, i_{N_{\mathrm{I}_j}(t)}\}.$$

Epidemiological processes

Immunity

In compartmental SIRS and SEIRS models, a concept of waning immunity and its impact on epidemics is associated with the rates at which individuals in class R revert back to class S. In agent-based SIRS and SEIRS models, we have the opportunity to consider the immunological history of individuals and, hence, can take a more refined approach to the complex process of how pathogens in an infector A_i are passed on the an infectee A_h. Here we model this as a probability generated from a concatenation of rates that include pathogen shedding by A_i, the survival of pathogens in the environment, whether contained in feces, urine, sweat, mucosal secretions or water droplets excreted by an infector, and a process whereby pathogens gain access to a host (entering through wounds, mucosal membranes or other membranes in the pulmonary or alimentary systems). We then characterize pathogen within-host strain replication rates in terms of pathogen mutational and reproductive processes. The final outcome in our model is either host recovery with some immunity or host death. We also consider the induction of host immunity through vaccination and make the assumption that waning immunity is the same, whether it stems from natural infection or vaccination. Of course, these may be modelled in different ways should data become available to make this distinction an important modeling

medRxiv preprint doi: https://doi.org/10.1101/2021.06.07.21258504; this version posted June 11, 2021. The copyright holder for this preprint (which was not certified by peer review) is the author/funder, who has granted medRxiv a license to display the preprint in perpetuity. All rights reserved. No reuse allowed without permission.

consideration.

Waning immunity. Recall that we use A_0 to denote an anonymous (generic) member of $\mathbf{S}$ and that A_i for $i > 0$ refers to a specific individual with an associated state list/vector. If some specific A_i is in immune state V_j having been infected with this strain at time τ_{ij}, we assume that the level of relative susceptibility of agent A_i to reinfection by strain j is given by (noting that the existence of the value τ_{ij} implies that infection of individual i by strain j at time τ_{ij} ensures that the V_j is no longer "null")

$$\omega_{ij}(t,\tau_{ij}) = \begin{cases} 0 & \text{if } \mathrm{V}_j \text{ is null} \\ \dfrac{1}{1+\left((t-\tau_{ij}-\sigma_{\mathrm{I}}-\sigma_{\mathrm{E}})/t_j^{\mathrm{half}}\right)^{\sigma}} & \text{if } t \geq \tau_{ij}+\sigma_{\mathrm{I}}+\sigma_{\mathrm{E}} \\ 1 & \text{if } t < \tau_{ij}+\sigma_{\mathrm{I}}+\sigma_{\mathrm{E}} \end{cases} \tag{A.6}$$

We note the following: 1.) the first case implies that τ_{ij} has yet to be defined; 2.) the second case is equivalent to the statement that $\tau_{ij} \geq 0$ now exists for strain j, since this occurs at time $t = \tau_{ij}$ (through the invocation of state $\mathrm{E}_j(t,\tau_{ij})$); 3.) $\omega_{ij}(t,\tau)$ ranges from 1 (i.e. full "on") at $t = \tau + \sigma_{\mathrm{I}} + \sigma_{\mathrm{E}}$ and decays to 0 as $t > \tau + \sigma_{\mathrm{I}} + \sigma_{\mathrm{E}} \to \infty$; 4.) agent i cannot be reinfected with its current major strain or with any other strain while it is currently itself in any state E_j or I_j for any $j = 0, ..., 2^J - 1$; 5.) the larger the value of σ the steeper or more abrupt the switch is from full immunity (equal to 1) at time τ through 1/2 at time t_j^{half} to approach 0 as $t \to \infty$ (we set $\sigma = 4$ as providing an intermediate level of abruptness).

Cross immunity with escape mutations. A somewhat more general implementation of cross-immunity may be based on the number of alleles by which strains j and ℓ differ. If they differ in k positions, then the level of cross immunity can be set to c^k. In this case

$$\text{Cascading } \mathbf{C}\text{:} \qquad c_{j\ell} = \begin{cases} 1 & \text{if } \ell = j \\ c^k & \text{if } \ell \text{ differs from } j \text{ by } k \text{ alleles and } \ell \end{cases} \tag{A.7}$$

In addition to this, one may also designate certain changes in certain alleles as "escape mutants" with respect to the progenitor strain. For these, the level of cross-immunity would be set to zero. Under these assumptions, a generalization of Eq. A.7 would be

$$\text{Escape mutation:} \qquad c_{j\ell} = \begin{cases} 1 & \text{if } \ell = j \\ c^k & \text{if } \ell \text{ differs from } j \text{ by } k \text{ alleles} \\ & \text{and } \ell \text{ is not an escape mutation} \\ 0 & \text{if } \ell \text{ is an escape mutation} \end{cases} \tag{A.8}$$

In particular, for the case $J = 7$, if strain $(1, x, x, x, x, x, x)$ is an escape mutation with respect to some level of immunity to strains $(0, x, x, x, x, x, x)$, then Eq. A.8 becomes

$$c_{j\ell} = \begin{cases} 1 & \text{if } \ell = j \\ 0 & \text{if } j \leq 63 \text{ and } \ell > 63 \\ c^k & \text{otherwise, where } \ell \text{ differs from } j \text{ by } k \text{ alleles} \end{cases} \tag{A.9}$$

medRxiv preprint doi: https://doi.org/10.1101/2021.06.07.21258504; this version posted June 11, 2021. The copyright holder for this preprint (which was not certified by peer review) is the author/funder, who has granted medRxiv a license to display the preprint in perpetuity. All rights reserved. No reuse allowed without permission.

Vaccination. A vaccine may be designed to give immunity to one or more particular identified strain j. Vaccination strategies include vaccinating at a fixed rate $v(t)$ (percent of individuals vaccinated at each time period) over a fixed period that begins at t_v^{on} and ends at t_v^{off} and can focus on drawing only on: i) individuals in the set **S**, ii) any non-infectious individual in **S** or **A**, or iii) any non-infectious, not previously vaccinated individual in **S** or **A**. The vaccine itself can be designed as follows:

- *Dominant strain vaccination at time* τ_{vac}. An individual S or A_i vaccinated with the dominant strain, say j, at time $\tau_{\text{vac}} \in [t_v^{\text{on}}, t_v^{\text{off}}]$ serves to add the disease state $\text{V}_j(t, \tau_{\text{vac}})$ to that individual's list. If the individual is already in state $\text{V}_j(t, \tau')$ at time $t > \tau_{\text{vac}}$, then its status is updated so that at time $t > \tau_{\text{vac}}$ it is now $\text{V}_j(t, \tau_{\text{vac}})$ rather than $\text{V}_j(t, \tau')$

- *Multi-strain vaccination at time* t_{vac}. An individual S or A vaccinated with a multi strain concoction at time $\tau \in [t_v^{\text{on}}, t_v^{\text{off}}]$, say with strain $j_1, \ldots, j_\nu$, will have their disease status updated with regard to all these strains, as in the dominant strain case.

Infectious contacts

Infectious individuals are assumed to make $\hat{\kappa}$ *effective contacts* each time period; where effective contacts are those that are sufficiently close and of a sufficiently long duration to constitute a "risk of transmission." This rate is either a constant κ_0, or in stochastic implementations drawn from a Poisson distribution with mean κ_0, or in adaptive formulations (e.g., under social distancing behaviour) is a function of the severity of the ongoing outbreak. We also assume at time t that under a random contact process, proportion $\frac{\hat{\kappa}(t)N_{\text{S}}(t)}{N_0 - N_{\text{D}}(t)}$ and $\frac{\hat{\kappa}(t)N_{\text{A}}(t)}{N_0 - N_{\text{D}}(t)}$ of these contacts will respectively be with susceptible and with uniquely identified agents, although only $\frac{\hat{\kappa}(t)(N_{\text{A}}(t) - N_{\text{E}}(t) - N_{\text{I}}(t))}{N_0 - N_{\text{D}}(t)}$ of those will be susceptible to infection with a new strain or reinfection with the same strain.

In the adaptive case, we assume $\kappa(t)$ decreases from κ_0 as the proportion of infectious individuals, $N_{\text{I}}(t)/(N_0 - N_{\text{D}}(t))$, increases such that $\kappa(t) = \kappa_0/2$ when $N_{\text{I}}(t)/(N_0 - N_{\text{D}}(t)) = p_{\text{I}}^{\text{half}}$. For convenience of implementation, however, we define the following "switching" (as apposed to hyperbolic) function

$$\kappa(t) = \begin{cases} \frac{\kappa_0}{1 + \left(\frac{N_{\text{I}}(t)}{N_0 - N_{\text{D}}(t)} \Big/ p_{\text{I}}^{\text{half}}\right)^2} & \text{when } p_{\text{I}}^{\text{half}} > 0 \\ \kappa_0 & \text{when } p_{\text{I}}^{\text{half}} = 0 \end{cases} \tag{A.10}$$

even though, from a continuity point of view, the top part of this expression implies that $\kappa(t) \to 0$ at $p_{\text{I}}^{\text{half}} \to \infty$.

Probability of infection

In deriving a probability $\pi_{ih,j\ell}^{\text{inf}}$ of an agent A_h being infected with strain ℓ by and agent A_i who is infectious with major strain j, we concatenate (i.e., multiply together) several process, each of which involves nominal constants. Thus, in all but one of these processes, the scaling of these constants can be normalized and given a relative set of values across strains though one set of

medRxiv preprint doi: https://doi.org/10.1101/2021.06.07.21258504; this version posted June 11, 2021. The copyright holder for this preprint (which was not certified by peer review) is the author/funder, who has granted medRxiv a license to display the preprint in perpetuity. All rights reserved. No reuse allowed without permission.

constants though relative, will ultimately all be scaled by fitting the model to real data. In our treatment below, constants associated with shedding and persistence will be scaled while those associated with within-host replication will be kept unscaled to be ultimately fitted to data. In particular, the parameters $\bar{\beta}_j$ associated with pathogen transmission (i.e., from contact to the start of within host replication—see Fig. 1) will be scaled by fitting to epidemiological data, while the relative values for the different strains regarding pathogen shedding and environmental persistence can be fitted to experimental data collect to set values of these processes when considered on their own.

Pathogen shedding. We assume that shedding is affected by the immune state of the infector A_i and thus posit the shedding rates below for this individual when its major infectious strain is j. In general, we have a matrix of shedding rates $\bar{\zeta}_{j\ell}$ before accounting for immunity and cross immunity that is specific to agent A_i. Immunity and cross-immunity act to reduce shedding rates through functions $\phi_{ij}(t) \in [0,1]$ that are computed in terms of A_i's waning functions ω_{im} with respect to strain m and a matrix of cross-immunity values c_{jm} that have been normalized so that $c_{jj} = 1$ for $j = 0, ..., 2^J - 1$ and $c_{jm} \in [0,1]$ for $j, m = 0, ..., 2^J - 1$. Specifically, we define agent-specific *immunity modifying functions*

$$\phi_{ij}(t) = \prod_{m=0}^{2^J-1} \big(1 - c_{mj}\omega_{im}(t)\big) \tag{A.11}$$

and assume that the shedding rates can be expressed as

$$\zeta_{ij\ell}(t) = \bar{\zeta}_{j\ell}\phi_{i\ell} \qquad \ell = 0, ..., 2^J - 1 \tag{A.12}$$

Environmental persistence. The persistence of pathogens in the environment are known to be impacted by humidity, temperature, airflow, and the surface properties of fomites [57]. This, and other factors relating the effects of weather on contact rates and efficacy, may result in overall pathogen transmission having a seasonal component to it [58]. In particular, viral persistence indoors may be much greater than outdoors, with a greater proportion of indoor contacts taking place during cold or wet weather. Thus the most appropriate place to introduce seasonal effects into epidemic processes is through contact rates and environmental persistence cycling over time with a period of one year (or even half-a-year if two comparatively spaced rainy seasons occur, as in some in tropical locations [59]) and an amplitude obtained by fitting parameters to data. Thus, in our model, we introduce constants $\bar{\eta}_\ell$, $\delta \in (0,1)$, k (appropriately scaled, depending on the units of time) and θ and assume that

$$\eta_\ell(t) = \bar{\eta}_\ell \left(1 + \delta \sin\left(\frac{2\pi t}{k} + \theta\right)\right) \qquad \ell = 0, ..., 2^J - 1 \tag{A.13}$$

The case $\delta = 0$ corresponds to constant values $\eta_\ell(t) = \bar{\eta}_\ell$ for all t, while if $\delta = 1$ we get the largest possible fluctuation between 0 and $2\bar{\eta}_\ell$. The constant k relates to the time units so we get one cycle per year, and θ shifts the cycle to set the points in time at which the maximum and minimum values of $\eta_\ell(t)$ occur.

medRxiv preprint doi: https://doi.org/10.1101/2021.06.07.21258504; this version posted June 11, 2021. The copyright holder for this preprint (which was not certified by peer review) is the author/funder, who has granted medRxiv a license to display the preprint in perpetuity. All rights reserved. No reuse allowed without permission.

Strain transmission. In the context of a standardized dose (which will be modified by multiplying the strain *effective contact* and transmission by both pathogen shedding and environmental persistence functions), the differential rates of strain transmission, which we denote by $\beta_{h\ell}$, will depend on a constant strain transmission rate parameter $\bar{\beta}_\ell$ modified by a function that represents the immune state of the infectee at time t: viz., recalling Eq. A.11

$$\beta_{h\ell}(t) = \bar{\beta}_\ell \phi_{h\ell}(t), \quad \ell = 0, ..., 2^J - 1 \tag{A.14}$$

Probability of infection. Using a competing rates formulation [60] to compute the probability of infection as a concatenation of the process of infector shedding (ζ), environmental persistence (η) and transmission rates (β), we obtain

$$\pi^{\text{inf}}_{ih,j\ell}(t) = \frac{\zeta_{ij\ell}(t)\eta_\ell(t)\beta_{h\ell}(t)}{\sum_{m=0}^{2^J-1} \zeta_{ijm}(t)\eta_m(t)\beta_{hm}(t)} \left(1 - e^{-\zeta_{ij\ell}(t)\eta_\ell(t)\beta_{h\ell}(t)}\right), \quad \ell = 0, ..., 2^J - 1 \tag{A.15}$$

Within-host processes

If after receiving an initial infectious dose of pathogen, an individual is infected primarily with strain ℓ, then we expect this strain to dominate unless intrinsic mutational processes are high (which is not the case for COVID-19) or the individual has some immunity to this dominant strain. In the latter case the situation is ripe for an "escape mutation," that is one that evades the immune system, to arise.

If we nominally set the relative rate at which an individual invaded by strain ℓ has an infection dominated by strain ℓ (i.e., ℓ in the terminology of [61] is the major strain of the infection) to be $(1 - \mu)$, then the probability that one of the other strains $\ell' \neq \ell$ (in the case of COVID we assume that $\mu > 0$ is very close to 0—e.g. of order 10^{-3} to 10^{-6}—while for viruses lacking error correcting machinery it can be considerably larger and of the order 10^{-1}). We can partition the latter probability according to a set of comparative strain within-host replication rates $\lambda_{\ell'}$, each moderated by its immune state function $\phi_{h\ell'}$ and a normalizing factor $\frac{1}{\sum_{\forall m \neq \ell} \lambda_m \phi_{hm}}$ to obtain

$$\pi^{\text{inv}}_{h\ell\ell'}(t) = \begin{cases} 1 - \mu & \text{for } \ell' = \ell \\ \mu \left(\frac{\lambda_{\ell'} \phi_{h\ell'}}{\sum_{\forall m \neq l} \lambda_m \phi_{hm}} \right) & \text{for } \ell' \neq \ell \end{cases} \tag{A.16}$$

Pathogen progression equations

Probability that infector A_i with major strain j will result in infectee A_h express ℓ' as its major strain is

$$\pi_{ih,j\ell'}(t) = \sum_{\ell=0}^{2^J-1} \pi^{\text{inf}}_{ih,j\ell}(t) \pi^{\text{inv}}_{h\ell\ell'}(t), \quad \ell = 0, ..., 2^J - 1 \tag{A.17}$$

medRxiv preprint doi: https://doi.org/10.1101/2021.06.07.21258504; this version posted June 11, 2021. The copyright holder for this preprint (which was not certified by peer review) is the author/funder, who has granted medRxiv a license to display the preprint in perpetuity. All rights reserved. No reuse allowed without permission.

Single strain case

In the single strain case ($J = 0$), the waning immunity equation Eq. A.6 reduces to (dropping the redundant index $j = 0$, and noting that the existence of a value τ_i implies A_i has been infected at time τ_i in the past)

$$\omega_i(t) = \begin{cases} 0 & \text{if } \mathrm{A}_i \text{ has never been infected} \\ \dfrac{1}{1 + \left((t - \tau_i - \sigma_\mathrm{I} - \sigma_\mathrm{E})/t^{\mathrm{half}}\right)^{\sigma}} & \text{if } t \geq \tau_i + \sigma_\mathrm{I} + \sigma_\mathrm{E} \\ 1 & \text{if } t < \tau_i + \sigma_\mathrm{I} + \sigma_\mathrm{E} \end{cases} \tag{A.18}$$

and the modifying immunity functions ϕ_{ij} (Eq. A.11) collapse to 1, which implies that the pathogen shedding functions $\bar{\zeta}_{i\ell}$ (Eq. A.12) collapse to 1. Without loss of generality, we can also assume that single strain value $\eta = 1$ in Eq. A.13, which implies that the probability of infection (Eq. A.15) reduces to

$$\pi_{ih}^{\mathrm{inf}}(t) = 1 - e^{-\bar{\beta}(1-\omega_h(t))} \tag{A.19}$$

Further, since in the single strain case there are no mutations to consider, it follows from Eq. A.16 that $\pi_{h\ell\ell'}^{\mathrm{inv}}(t) = 1$ for all h and we finally have that $\pi_{ih}(t) = \pi_{ih}^{\mathrm{inf}}(t) = 1 - e^{-\bar{\beta}(1-\omega_h(t))}$ (Eq. A.17) for all h.

Simulation algorithm

1. **Parameters selected at the start of a simulation**
   (a) N_0: Number of individuals in the population. Assumed to be fixed over time (i.e., the population is closed), but partitioned into sets **S**, **A** and **D** with respectively $N_\mathrm{S}(t)$, $N_\mathrm{A}(t)$ and $N_\mathrm{D}(t)$ individuals in each set and satisfying Eq. A.1.
   (b) J: The $\log_2$ of the number of possible strains indexed by $j = 0, \cdots, 2^J - 1$
   (c) $\bar{\beta}_j$: Strain dependent transmission parameters (the process between contact and the start of strain replication and nominally equivalent to transmission in SEIR models—see Fig. 1) for pathogen strain j
   (d) t_j^{half}: The time it takes for immunity to strain j to have waned by half.
   (e) σ_{E_j}: The time it takes from initial infection for an infected individual to become more likely to become infectious than remain infected without being infectious.
   (f) σ_{I_j}: The additional time it takes beyond σ_{E_j} for an infectious individual to more likely transition beyond being infectious than remain infectious.
   (g) p_{α_j}: The proportion of individuals leaving the infectious category that die, which implies that $1 - p_{\alpha_j}$ is the proportion that become immune.
2. **Initialization**

medRxiv preprint doi: https://doi.org/10.1101/2021.06.07.21258504; this version posted June 11, 2021. The copyright holder for this preprint (which was not certified by peer review) is the author/funder, who has granted medRxiv a license to display the preprint in perpetuity. All rights reserved. No reuse allowed without permission.

(a) Set up pathogen list (see Eq. A.2)

(b) Initialize the simulation by setting $t = 0$ and creating the agent list $\mathbf{A}(0)$ one infectious and $N_0 - 1$ susceptible agents.

3. **Time t: vaccination loop.**

   (a) Carry out the vaccination process before going into the rest of the loops with the updated S and A sets after the vaccinations.

4. **Time t: contact loop.** Set up contacts for the current round of encounters at time t (i.e., the inner agent-driven contact loop within the outer time-driven loop) and tag for outer loop update of disease status, as follows:

   (a) *Numbers in various sets and associated index sets.* Identify the number of individuals $N_{\mathrm{S}}(t)$, $N_{\mathrm{A}}(t)$ and $N_{\mathrm{D}}(t)$ in sets $\mathbf{S}$, $\mathbf{A}$ and $\mathbf{D}$ at time t respectively, as well as the number of exposed (but not yet infectious) agents $N_{\mathrm{E}}(t)$, infectious agents $N_{\mathrm{I}}(t)$ and identified non-infected agents $N_{\mathrm{A_S}}(t) = N_{\mathrm{A}}(t) - N_{\mathrm{I}}(t) - N_{\mathrm{E}}(t)$. Break down the infectious agents tally into the number of agents N_{I_j} infectious with strain $j = 0, 1, ..., 2^J - 1$. We will also need the index sets $\mathbb{I}_{\mathrm{A_S}}$ and $\mathbb{I}_{\mathrm{I}_j}(t)$, $j = 0, ..., 2^J - 1$ at time t.

   (b) *Infectious contacts with each group.* The rate at which any individual contacts other individuals per unit time is given by the contact rate parameter $\kappa > 0$. Assuming random contact events over one unit of time, the actual number of individuals that agent A_i contacts at time t is then given by

$$\hat{\kappa}_i(t) \sim \texttt{POISSON}[\text{mean} = \kappa(t)]$$

   Of these, proportions

$$\pi_{i\mathrm{S}} = \frac{N_{\mathrm{S}}(t)}{N_0 - N_{\mathrm{D}}(t)} \tag{A.20}$$

   and

$$\pi_{i\mathrm{A}} = \frac{N_{\mathrm{A}}(t) - N_{\mathrm{I}}(t) - N_{\mathrm{E}}(t)}{N_0 - N_{\mathrm{D}}(t)} \tag{A.21}$$

   are expected to come from susceptibles in the sets $\mathbf{S}(t)$ and $\mathbf{A}_{\mathrm{S}}(t)$ (see Eq. A.5) respectively. Thus the actual number of contacts in set $\mathbf{S}(t)$, $\mathbf{A}_{\mathrm{S}}(t)$, and $\mathbf{E}(t) \cup \mathbf{I}(t)$ are

$$\left(\hat{N}_i^{\mathrm{S}}(t), \hat{N}_i^{\mathrm{A_S}}(t), \hat{N}_i^{\mathrm{E}}(t) + \hat{N}_i^{\mathrm{I}}(t)\right) = \texttt{Multinomial}\left[\hat{\kappa}_i; \pi_{i\mathrm{S}}, \pi_{i\mathrm{A}}, 1 - \pi_{i\mathrm{S}} - \pi_{i\mathrm{A}}\right] \tag{A.22}$$

   We note that only $\hat{N}_i^{\mathrm{S}}(t)$ and $\hat{N}_i^{\mathrm{A_S}}(t)$ are of interest because individual in states E and I cannot be reinfected. Also, we make the assumption below that the first infection that an individual in set $\mathbf{A}$ contracts in this contact loop, is the one that counts (i.e., there will

medRxiv preprint doi: https://doi.org/10.1101/2021.06.07.21258504; this version posted June 11, 2021. The copyright holder for this preprint (which was not certified by peer review) is the author/funder, who has granted medRxiv a license to display the preprint in perpetuity. All rights reserved. No reuse allowed without permission.

be no simultaneously infections with multiple strains). Finally, since contacting individuals is tantamount to sampling with replacement, the number of unique contacts (i.e., all multiple contacts are counted as a single contact) that agent A_i has with individuals in the set $\mathbf{S}$ is $\hat{N}_i^{\mathrm{S}}(t)$ reduced by excluding multiple contacts (which under a random contact model is a negative exponential correction) to obtain

$$N_i^{\mathrm{S}*}(t) = \min\left\{\hat{N}_i^{\mathrm{S}}(t), \texttt{Binomial}\left[\hat{\kappa}_i(t), e^{-\hat{\kappa}_i(t)/\hat{N}_i^{\mathrm{S}}(t)}\right]\right\} \tag{A.23}$$

Thus if $\hat{\kappa}_i(t) << \hat{N}_i^{\mathrm{S}}(t)$, $N_i^{\mathrm{S}*}(t)$ is expected to be very close to the upper value $\hat{\kappa}_i(t)$. On the other hand, if $\hat{\kappa}_i(t) \approx \hat{N}_i^{\mathrm{S}}(t)$, then $N_i^{\mathrm{S}*}(t)$ is expected to be around $\hat{\kappa}_i(t)/e \approx 0.37\hat{\kappa}_i(t)$. Additionally, after dealing with each agent i reduce in the size of $N_{\mathrm{S}}(t)$ to take account of those agents that had been infected by agent A_i and had now entered the ranks of the set $\mathbf{A}$.

(c) *Identify all infectious agents and their pathogens strains.* Among all agents in the set $\mathbf{A}(t)$ (Eq. A.4), identify those that have an infectious strain I_j for some $j = 0, \cdots, 2^J - 1$. Thus, if the number of infectious agents with infectious strain j is $N_{\mathrm{I}_j(t)}$ then consider the set

$$\mathbf{I}_j(t) = \{\mathrm{A}_{i_1}^j(t), \mathrm{A}_{i_2}^j(t), \ldots, \mathrm{A}_{N_{\mathrm{I}_j}}^j(t)\}$$

with index set

$$\mathbb{I}_{\mathrm{I}_j}(t) = \{i_{1_j}, \cdots, i_{N_{\mathrm{I}_j}(t)}\}$$

Initially, most of these sets will be empty, but will fill in over time.

(d) *Susceptible contacts.* The probability that an agent A_i with a strain j major infection infects a susceptible (nominally denoted by individuals of type A_0) who then becomes infectious with dominant strain ℓ' is given by the probability $\pi_{i0,j\ell'}$ computed in Eq. A.17, which itself relies on expressions Eq. A.10-A.16. The actual number of individuals in the set $\mathbf{S}$ will make effective contact with one more infectious individuals is $N_i^{\mathrm{S}*}(t)$ obtained using Eq. A.23. Thus, from a multinomial drawing, we can now generate the number of newly exposed individuals, $N_{0\ell'}^{\mathrm{E}+}(t+1)$ (the "+" is used to denote these are newly added and the "0" that they are coming from the set $\mathbf{S}$), with major strain ℓ' at time $t+1$, have been infected by agent A_i with major pathogen strain j on the time interval $[t, t+1)$:

$$\begin{aligned}(\hat{N}_{00}^{\mathrm{E}+}(t), \cdots, \hat{N}_{02^J-1}^{\mathrm{E}+}(t)) \quad &\sim \\ &\texttt{Multinomial}\left[N_i^{\mathrm{S}*}(t); \pi_{i0,j0}(t), \cdots, \pi_{i0,j\,2^J-1}(t)\right]\end{aligned} \tag{A.24}$$

These individuals will be used to update list of currently infected individuals in the sets $\mathbf{A}_{\mathrm{E}_j}$, $j = 0, ..., 2^J - 1$ at time t+1, which is computed in the outer loop computation, as presented below. We also note that the probabilities in the above multinomial add to less than 1, so that at the end of the drawing a proportion of the individuals $N_i^{\mathrm{S}*}(t)$ remain uninfected.

medRxiv preprint doi: https://doi.org/10.1101/2021.06.07.21258504; this version posted June 11, 2021. The copyright holder for this preprint (which was not certified by peer review) is the author/funder, who has granted medRxiv a license to display the preprint in perpetuity. All rights reserved. No reuse allowed without permission.

(e) *Agent contacts.* The number of agents $\hat{N}_i^{\mathrm{A_S}}(t) \in \mathbb{I}_{\mathrm{A}\setminus(\mathrm{E}\cup\mathrm{I})}$ that come into contact with agent A_i over the interval $(t, t+1)$ is given by Eq. A.22. This number is drawn from the set $\mathbb{I}_{\mathrm{A}\setminus(\mathrm{E}\cup\mathrm{I})}$ with replacement and the following multinomial computation is used to determine how to update agent A_h at time $t+1$ when coming into contact with agent A_i on the interval $(t, t+1)$ using the probabilities of transmission given in Eq. A.17. Specifically, agent A_h will become infected with major strain ℓ' at time $t+1$ is determined by the multinomial drawing

$$\mathrm{A}_h \in \mathbf{A}_{\mathrm{E}_j} \text{ for some } j \sim \texttt{Multinomial}\left[1; \pi_{ih,j0}(t), \cdots, \pi_{ih,j\,2^J-1}(t)\right] \tag{A.25}$$

We note here that since the agents $A_h,\ h \in \mathbb{I}_{\mathrm{A}\setminus(\mathrm{E}\cup\mathrm{I})}$ are drawn with replacement as the computation proceeds and the agents $\mathrm{A}_i,\ i \in \mathbb{I}$ are cycled through, if a previously drawn A_h is drawn again, but has already been infected in the current round then we ignore the latest event, but keep the previous infection event intact. To obviate bias in this procedure, we need cycle through the agents $\mathrm{A}_i, i \in \mathbb{I}$ at random rather than in numerical order.

5. **Time t: disease progression loop.**

(a) *Individuals in $\mathbf{A}_{\mathrm{E}}$ at time t.* An individual $\mathrm{A}_i \in \mathbf{A}_{\mathrm{E}}$ at time t and in state $\mathrm{E}_j(t, \tau_i)$, $j = 0, ..., 2^J - 1$, becomes either an individual in state $\mathrm{E}_j(t+1, \tau_i)$ with probability

$$\pi_{\mathrm{E}_j}(t) = \frac{1}{1 + \left(\frac{t-\tau_i}{\sigma_{\mathrm{E}_j}}\right)^4} \tag{A.26}$$

or transfers to state $\mathrm{I}_j(t+1, \tau_i)$ with probability $\left(1 - \pi_{\mathrm{E}_j}(t)\right)$ thereby entering class $\mathbf{A}_{\mathrm{I}}$ at time $t+1$.

(b) *Individuals in $\mathbf{A}_{\mathrm{I}}$ at time t.* An individual $\mathrm{A}_i \in \mathbf{A}_{\mathrm{I}}$ at time t and in state $\mathrm{I}_j(t, \tau_i)$, $j = 0, ..., 2^J - 1$, becomes either an individual in state $\mathrm{I}_j(t+1, \tau_i)$ with probability

$$\pi_{\mathrm{I}_j}(t) = \frac{1}{1 + \left(\frac{t-\tau_i}{\sigma_{\mathrm{E}_j}+\sigma_{\mathrm{I}_j}}\right)^4} \tag{A.27}$$

or leaves the set $\mathrm{I}_j(t+1, \tau_i)$ with probability $\left(1 - \pi_{\mathrm{I}_j}(t)\right)$. In this latter case, the individual either dies with probability p_{α_j} or enters the state $\mathrm{V}_j(t+1, \tau_i)$ at time $t+1$ with probability $1 - p_{\alpha_j}$ The total number of individuals dying over the interval $[t, t+1)$ is noted as having a value $\Delta N_{\mathrm{D}}(t)$.

6. **Time $t+1$: outer loop update.** The outer loop records all the events that took place in the contact and disease progression loops and updates the agents state at the next time step. It also updates all other states as follows.

medRxiv preprint doi: https://doi.org/10.1101/2021.06.07.21258504; this version posted June 11, 2021. The copyright holder for this preprint (which was not certified by peer review) is the author/funder, who has granted medRxiv a license to display the preprint in perpetuity. All rights reserved. No reuse allowed without permission.

(a) *Individuals in* $\mathbf{A}_{\mathrm{S}}$ *at time* t. For the $N_{\mathrm{S}}(t)$ individuals in $\mathbf{A}_{\mathrm{S}}$ at time t, we have $N_{0j}^{\mathrm{E}+}(t)$ enter set $\mathbf{A}_{\mathrm{E}_j}(t+1)$ and we update

$$N_{\mathrm{S}}(t+1) = N_{\mathrm{S}}(t) - \sum_{j=0}^{2J-1} N_{0j}^{\mathrm{E}+}(t)$$

where Eq. A.23 ensures that $N_{\mathrm{S}}(t+1) \geq 0$

(b) *Individuals in* $\mathbf{A}_{\mathrm{S}}$ *that are infected again over* $[t, t+1)$. These individuals can become reinfected as calculated in the contact loop. Those that become reinfected with strain j, $j = 0, ..., 2^J - 1$ enter state $\mathbf{E}_j(t+1, t+1)$ at time $t+1$.

(c) *Updating the immunity of individuals in* $\mathbf{A}_{\mathrm{S}}$. Every individual within $\mathbf{A}_{\mathrm{S}}$ at time t must have its immunity status updated so that for $j = 0, ..., 2^J - 1$, if A_i is in state $\mathrm{V}_j(t, \tau_{ij})$ at time t then it transfers to state $\mathrm{V}_j(t+1, \tau_{ij})$ at time $t+1$, even if reinfected, as in b.) above.

(d) *Transfer from* $\mathbf{S}$ *to* $\mathbf{A}$. The $\hat{N}_{0j}^{\mathrm{E}}(t)$ computed in Eq. A.24 become newly listed members of the set $\mathbf{A}$ by entering state $\mathbf{E}_j(t+1, t+1)$, $j = 0, ..., 2^J - 1$. This involves updating the equations for $N_{\mathrm{S}}(t)$ and $N_{\mathrm{A}}(t)$, including taking account of the number of individuals $\Delta N_{\mathrm{D}}(t)$ that died from the disease in the immediate time period, i.e.:

$$\begin{aligned} N_{\mathrm{S}}(t+1) &= N_{\mathrm{S}}(t) - \sum_{j=0}^{2^J-1} \hat{N}_{0j}^{\mathrm{E}}(t) \\ N_{\mathrm{A}}(t+1) &= N_{\mathrm{A}}(t) + \sum_{j=0}^{2^J-1} \hat{N}_{0j}^{\mathrm{E}}(t) - \Delta N_{\mathrm{D}}(t) \\ N_{\mathrm{D}}(t+1) &= N_{\mathrm{D}}(t) + \Delta N_{\mathrm{D}}(t) \end{aligned} \tag{A.28}$$

(e) Along with input parameter values $t_{\mathrm{vac_on}} \geq 0$, $t_{\mathrm{vac_off}}$ and $p_v \in [0, 0.1]$, we also need to specify the valency of the vaccination by selecting 1 to 4 numbers that take on values $0, ..., 2^J - 1$ (if more valencies are needed than 4, then the platform needs to be modified accordingly). We also need specify whether N_{select} will just be individuals in the set $\mathbf{S}(t)$ ($N_{\mathrm{select}} = N_{\mathrm{S}}$) or will be any individual other than those in the set $\mathbf{A}_{\mathrm{I}}(t)$ ($N_{\mathrm{select}} = N_{\mathrm{S}} + N_{\mathrm{A}} - N_{\mathrm{I}}$).

In Algorithm 1 we summarise the steps of the simulation algorithm, as described in this section. On the right we report the name and numbering of the subsections while in the for loops we list the various steps respecting the item letters. Note that technical steps not explicitly described in the text (e.g. store updates, store set progression) do not present letters or numbers. The time set is defined with T while to describe temporal progression of set $\mathbf{S}, \mathbf{A}$ and $\mathbf{D}$ we use the symbols $\mathcal{S}, \mathcal{A}, \mathcal{D}$ respectively.

Estimation of R_0.

In a continuous time, SEIR model, when κ is folded into an all encompassing frequency-dependent transmission rate parameter $\beta_\kappa = \beta\kappa > 0$ (i.e.,

medRxiv preprint doi: https://doi.org/10.1101/2021.06.07.21258504; this version posted June 11, 2021. The copyright holder for this preprint (which was not certified by peer review) is the author/funder, who has granted medRxiv a license to display the preprint in perpetuity. All rights reserved. No reuse allowed without permission.

Algorithm 1: Summary of simulation algorithm

input N_0, J, $\bar{\beta}_j$, t_j^{half}, σ_{E_j}, σ_{I_j}, p_{α_j}, $j = 0, ..., 2^J - 1$ `// 1)`
`parameters`
$\{(\bar{\eta}_j, \bar{\beta}_j, \lambda_j, p_{\alpha_j};\ \zeta_{jm}$ and c_{jm} for $m = 0, ..., 2^J - 1)$ `// 2a) pathogen`
$\mid j = 0, ..., 2^J - 1\}$ `// list`
$t = 0, N_{\text{I}}(0) = 1, N_{\text{S}}(0) = N_0 - 1$ `// 2b) initialization`
for t *in* T **do**
  if $N_{\text{I}} > 0$ **then**
    for *agent in* $\mathbf{S} \cup (\mathbf{A} \setminus \mathbf{I})$ **do** `// 3) vaccination loop`
      3a) Vaccination process
      Update N_{S} and N_{A}
    for *agent in* $\mathbf{I}$ **do** `// 4) contact loop`
      4a) Numbers in various sets and associated index sets
      4b) Infectious contacts with each group
      4c) Identify all infectious agents and their pathogens strains
      4d) Susceptible contacts
      4e) Agent contacts
      Store updates
    for *agent in* $\mathbf{E}$ **do** `// 5a) disease progression loop`
      5a) Individuals in $\mathbf{A}_{\text{E}}$ at time t
      Store updates
    for *agent in* $\mathbf{I}$ **do** `// 5b) disease progression loop`
      5b) Individuals in $\mathbf{A}_{\text{I}}$ at time t
      Store updates
    Updates from loops 4), 5a) and 5b)
    6a) Individuals in $\mathbf{A}_{\text{S}}$ at time t `// 6) updates in outer loop`
    6b) Individuals in $\mathbf{A}_{\text{S}}$ that are infected again over $[t, t+1)$
    6c) Updating the immunity of individuals in $\mathbf{A}_{\text{S}}$
    6d) Transfer from $\mathbf{S}$ to $\mathbf{A}$
    6e) Specify the valency of the vaccination
    $\mathcal{S}[t] \leftarrow \mathbf{S}(t)$ `// store set progression`
    $\mathcal{A}[t] \leftarrow \mathbf{A}(t)$
    $\mathcal{D}[t] \leftarrow \mathbf{D}(t)$
return $\mathcal{S}, \mathcal{A}, \mathcal{D}$

medRxiv preprint doi: https://doi.org/10.1101/2021.06.07.21258504; this version posted June 11, 2021. The copyright holder for this preprint (which was not certified by peer review) is the author/funder, who has granted medRxiv a license to display the preprint in perpetuity. All rights reserved. No reuse allowed without permission.

total is transmission given by $\frac{\beta SI}{N}$ [49, 50]), $\gamma > 0$ is the transition rate from E to I and $\rho > 0$ is recovery rate from I to R, then R_0 corresponds to [62]

$$R_0 = \frac{\beta_\kappa}{\gamma + \rho} \tag{A.29}$$

B J-RAMP Details

General description

The J-RAMP design augments a desktop simulation platform with several novel features that increase flexibility and expressiveness, and promote experimentation and interoperability with other platforms. These include an API ("application programming interface") fully supporting remote operation and direct retrieval of data for external processing on other platforms, such as Python, Javascript or the R statistical platform. The API can also be accessed by an onboard scripting interface that uses the Nashorn Javascript engine.

Additionally, using a novel design, elements of the internal algorithm are exposed for possible reprogramming in a secure fashion that will not damage the overall system. These runtime alternative modules (RAMs) may also be controlled from the API to facilitate selective algorithm redefinition during the run of the simulation.

Use of the J-RAMP features require some experience with scripting and/or Java coding, however the resulting modifications to the algorithm can be of great significance. The RAM platform is implemented to support program redefinition with no risk to damaging the underlying code base. It should be accessible to anyone with moderate scripting experience.

A major goal of the J-RAMP project is to pre-package these functionalities so that they can be readily deployed as part of simulation system design. This goal has been partially realized with respect to the RAM platform: annotations can be added to the simulator's source code that direct the automatic generation of Java code to integrate into the simulations's source and provide the functionality.

The following discussion assumes some familiarity with script or program development.

Runtime alternative modules

Figure B.1 shows the RAM redefinition frame. The available RAMs appear as radio buttons along the bottom of the frame. Each RAM is a set of options for defining a relatively short Java method implementing some key aspect of the simulation algorithm. For example, included in this simulation are the implementation for cross immunity given in Eq. 1; the implementation for β given in Eq. A.14; and the implementation for ϕ given in Eq. A.11; etc. Each RAM initially contains only a single option, Option 0, the default, internally defined implementation. Option 0 cannot be edited and appears for reference purposes only.

Additional options may be added to each RAM containing code redefining the method. Two editor panes and one console pane are stacked in the frame

medRxiv preprint doi: https://doi.org/10.1101/2021.06.07.21258504; this version posted June 11, 2021. The copyright holder for this preprint (which was not certified by peer review) is the author/funder, who has granted medRxiv a license to display the preprint in perpetuity. All rights reserved. No reuse allowed without permission.

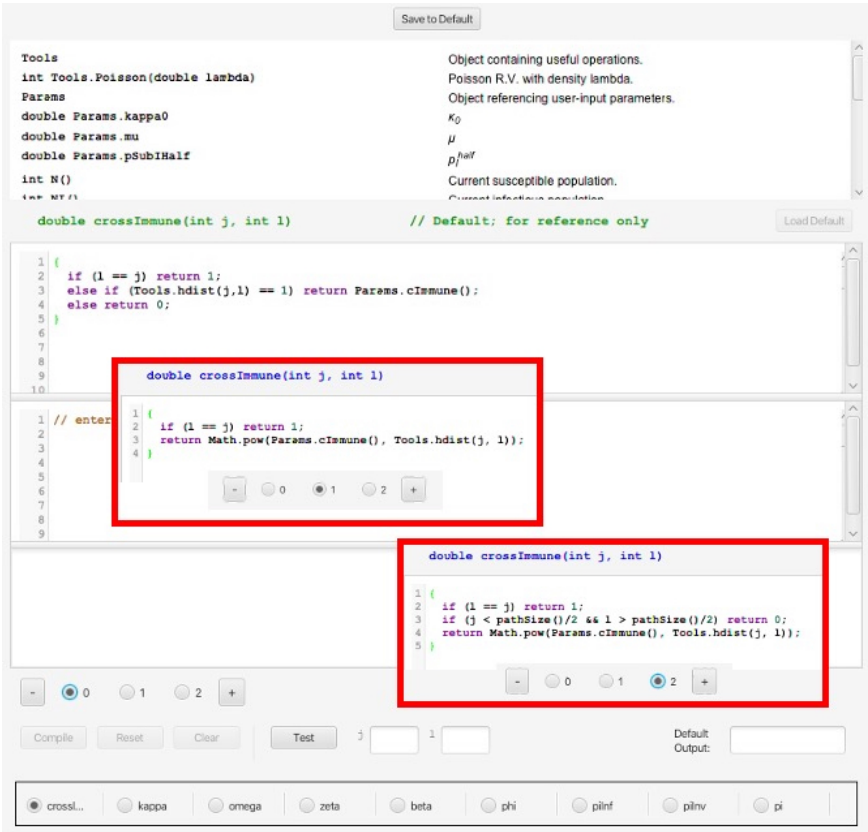

Figure B.1: RAM frame shows the implementation of the nearest-neighbor cross-immunity formulation **C** of Eq. 1 as the default. In the red-bordered insets are the cascading cross-immunity with escape mutation formulations of Eqs. A.7 and A.9. Note the radio-buttons are set to 0 in the main figure and to 1 and 2 in the insets. Also note the "+" button which allows for an unlimited number of alternatives to be set up using consecutive integer numbers for the new radio-buttons that appear and pertain to the selection of each alternative. Note at the bottom the list of functions that can be altered at runtime. The "load default" button on the upper left hand side allows the user, when starting a new alternative, to insert the default code (which is immutable in radio-button 0) as a starting point. The frame also documents a list of terms in the upper panel that can be used to build any function.

and display the code and output of the RAM. These panes show the content associated with the currently selected RAM and option. The top editor pane contains the code for the method being redefined. The second editor pane contains definitions of any new help functions required by the definition in the top pane. The console pane contains messages and output that are useful during the development of the option. For convenience, a "Load Default" button initializes the editor to an editable version of the Option 0 default to use as a starting point.

Figure B.1 shows the Option 0 default definition for the cross immunity

medRxiv preprint doi: https://doi.org/10.1101/2021.06.07.21258504; this version posted June 11, 2021. The copyright holder for this preprint (which was not certified by peer review) is the author/funder, who has granted medRxiv a license to display the preprint in perpetuity. All rights reserved. No reuse allowed without permission.

matrix function, as described by Eq. 1. Clicking the "+" button produced two new options, which appear in the insets. These option implement the alternative cascading cross immunity schemes presented in Eqs. A.7 and A.9. Option 2 code appears below:

```
    double crossImmune(int j, int k)  {
        if (l == j) return 1;
        if (j < pathSize()/2 && l > pathSize()/2) return 0;
        return Math.pow(Params.cImmune(), Tools.hdist(j, l));
    }
```

Note that we have substituted the function `pathSize` for a hard-coded value of 63. `pathSize` returns the number of pathogens, allowing us to use this formulation for any choice of entropy. Documentation for `pathSize` is at the top of the window in the list of available help functions and parameters. There is also more extensive documentation in a separate user guide (see Fig. B.2).

The platform duplicates a mini-development environment for building alternative definitions. Once code has been entered the "Compile" button checks the legality of the code and makes it available for use at runtime. Legally compiled code will produce a "Compilation Successful" message. Errors will appear with line numbers if they occur. Once the code is legal, the "Test" button can be used with actual parameters entered into the small text fields to determine correctness of the code. It is also possible to include `print` and `println` statements in the code during development to further check correctness. Output from print statements will appear in the bottom console window. The entire RAM set can be saved and will reappear during subsequent launches of the simulator platform.

To use an alternate RAM definition at runtime simply select the desired option. (Selected options will be restored from a saved RAM set during subsequent launches.) The system will compile any uncompiled code the first time it is accessed. If an error occurs during a runtime compilation an alert will notify the user that the system is returning to the default definition of that RAM. At no time is the internal logic of the program overridden.

Finally, RAM option selection is part of the API described in the next section. This means that a script may run a simulation selecting different options at different points in time, using logic that considers the state of the model. For example, such an adaptive protocol might be appropriate for determining the contact rate κ.

Application programming interface

The API is a simple bytecode[1] called BPL (Blackbox Programming Language) that addresses all available user interactions with the simulator. Instructions fall into three categories: parameter assignment and retrieval; simulator operation; and data retrieval. A complete list of instructions is shown in Fig. B.3. Instructions are comprised of opcodes (e.g., `reset`, `step`, `get`) followed by 0 or more arguments. Every BPL operation returns a result, even if empty, for

[1] a *bytecode* is computer source code that is processed immediately by a program, usually referred to as an interpreter or virtual machine.

medRxiv preprint doi: https://doi.org/10.1101/2021.06.07.21258504; this version posted June 11, 2021. The copyright holder for this preprint (which was not certified by peer review) is the author/funder, who has granted medRxiv a license to display the preprint in perpetuity. All rights reserved. No reuse allowed without permission.

J-RAMP SEIVD IBM A-Mod Guide

rms wgetz

May 2021

ω (Equation 9)

$$\omega_{ij}(t) = \begin{cases} 0 & \text{if } \mathrm{V}_j \text{ is null} \\ \dfrac{1}{1 + \left((t - \tau_{ij} - \sigma_{\mathrm{I}} - \sigma_{\mathrm{E}})/t_j^{\mathrm{half}}\right)^{\sigma}} & \text{if } t \geq \tau_{ij} + \sigma_{\mathrm{I}} + \sigma_{\mathrm{E}} \\ 1 & \text{if } t < \tau_{ij} + \sigma_{\mathrm{I}} + \sigma_{\mathrm{E}} \end{cases}$$

Code

```
double omega(int i, int j)
{
  if (i == 0) return 0.0;        // Special case; A_0 never infected
  InfectedAgentState astate = getStateOf(i, j);
  if (astate == null || !(astate instanceof V)) return 0.0;
  double tau =  tau(i,j);
  double sigI = sigmaI(j);
  double sigE = sigmaE(j);
  double timeSinceInfect = tau + sigI + sigE;
  if (time() <= timeSinceInfect) return 1.0;
  return 1/(1 + Math.pow((time() - timeSinceInfect)/tHalf(j), Params.sigma()));
}
```

Notes

`astate = getStateOf(i,j)`	`astate` is assigned to a Java `InfectedAgentState` object for agent i with respect to pathogen j. `InfectedAgentState` objects can either be state `E`, `I`, `V` or `null` (the latter for never-infected or dead agents.)
`astate == null || !(astate == V)`	`astate` is something other than state `V`.
`tau(i,j)`	$= \tau_{ij}$.
`sigmaI(j)`	$= \sigma_{\mathrm{I}}$.
`sigmaE(j)`	$= \sigma_{\mathrm{E}}$.
`tHalf(j)`	$= \tau_j^{half}$.
`time()`	$= t$.
`Params.sigma()`	$= \sigma$.

Figure B.2: A description from our User Guide of the immunity waning function ω.

synchronization purposes. A string consisting of a sequence of opcodes and arguments may be submitted to the BPL interpreter, an example of which is shown in the notes in Fig. B.3.

Parameter assignment and retrieval. Every user-configurable element (including random number generator seeds) is addressed from BPL using a unique three-letter "airport code" (see Table. B1). Additionally, pathogens are addressed by their id number (0 to $2^J - 1$) and agent states using identifiers S, E, I, V, DI+ and DD (the latter two represent ΔI and ΔD, respectively). RAM options are addressed in `setOption` and `getOption` using the name of the RAM (e.g., "crossImmune"). Get and set operations can be used on each of these with the exception of ENT (strain entropy), which is read-only.

medRxiv preprint doi: https://doi.org/10.1101/2021.06.07.21258504; this version posted June 11, 2021. The copyright holder for this preprint (which was not certified by peer review) is the author/funder, who has granted medRxiv a license to display the preprint in perpetuity. All rights reserved. No reuse allowed without permission.

Simulator operation. Simulation runs begin by executing the BPL `reset` instruction, followed by **step**, **run_for** or **run**. The BPL interpreter operates synchronously with the simulator by waiting to process subsequent commands during a simulation run. Operational instructions can be interspersed with parameter set/get or data retrieval to use in runtime decision-making. Note that the **reset** operation restores the simulator to its state at the time of the last **reset**, so that no parameter changes made during a run are persistent.

Data retrieval Operations to obtain the current population in each state, and to retrieve the runtime population history of each state and pathogen are also included. These can be easily transformed into R data frames, for example, for further analysis.

Scripting can be deployed using either one of the two on-board script interpreter interfaces, or remotely from another platform using drivers provided with the simulator. The remote drivers use an operating system channel called *named pipes* or *fifos* that are part of all MacOS, Windows, Linux, and other Unix^{TM}-based systems.

On our main dashboard, we provide two scripting windows that are opened using the "S On" and "JS On" buttons (see button second and third from left at bottom of Fig. 2A). The former allows the user to write simulation driver scripts directly as command strings. (The commands listed in Fig. B.3 are accessed by pressing the "Command Reference" button in the "S On" window.) This window is used primarily to test and monitor scripts intended to be deployed on a remote platform. The JS window contains a Nashorn Javascript interpreter enhanced to accept and execute BPL operations. Scripts can developed, saved, and used to drive the simulator from this interpreter. For example, Fig. B.4, lists the code used to implement the adaptive vaccination programs. The `SEIV` object referenced in this code contains methods corresponding to the BPL operations detailed in Fig. B.3.

Table B1: Airport codes for parameter and variables used in the model algorithm

Name	Math	Code	Name	Math	Code
		Epidemic codes			
% mortality	p_α	MOR	transmission	β	XMT
env. persist.	η	PST	within-host replication	λ	INV
median latent period	σ_{E}	MLP	median infectious period	σ_{I}	MIP
population size	N_0	POP	contact rate	$\bar{\kappa}$	CPT
mutation rate	μ	MUR	abruptness of waning	σ	AOW
cross immunity	c	CIM	waning half-life	t^{half}	WHA
seas. trans. peturb	δ	STP	seas. trans. shift	θ	STS
seas. trans. period	k	PER	adap. contact param.	$p_{\mathrm{I}}^{\mathrm{half}}$	IPC
strain entropy	J	ENT	shedding rate	$\bar{\zeta}$	SHD
		Vaccination codes			
enable vaccination		VEN	vaccine on/off	$t_v^{\mathrm{on}}/t_v^{\mathrm{off}}$	VOO
strain valency type	VA#, #=1,..,4		selection composition		VCP
vaccinate susc. only		VSU	vaccinate non-infectious		NVI
vaccinate non-vacc.		VNV			

medRxiv preprint doi: https://doi.org/10.1101/2021.06.07.21258504; this version posted June 11, 2021. The copyright holder for this preprint (which was not certified by peer review) is the author/funder, who has granted medRxiv a license to display the preprint in perpetuity. All rights reserved. No reuse allowed without permission.

BPL Reference

Commands

`reset`	Resets simulation with initial slider/switch values.
`restart`	Resets simulation with current slider/switch values.
`run_for T`	Run the simulation from the current time for *T* steps.
`run`	Run the simulation for the number of steps set by the last `run_for` command.
`step`	Single-step the simulation one time unit.
`get time`	Returns current simulation time.
`getLimit XXX`	Returns lower and upper values of limit control labeled *XXX* on separate lines.
`getPath XXX id`	Returns value of parameter *XXX* in pathogen *id*.
`get XXX`	Returns value of non-limit control labeled *XXX*.
`setLimit XXX lo hi`	Sets the limit control *XXX* to limits *lo hi*.
`setPath XXX id Y`	Sets value of parameter *XXX* in pathogen *id* to *Y*.
`set XXX Y`	Sets value of non-limit control *XXX* to *Y*.
`pathPop id Z`	*id* is a pathogen id and *Z* must be one of the agent state identifiers (S, E, I, V, DI+, DD). Returns the current population in state *Z* with respect to pathogen *id*.
`totPop Z`	*Z* must be one of the agent state identifiers (S, E, I, V, DI+, DD). Returns the total population in state *Z*.
`timeTrail`	Returns the array of timesteps for use in a table with other trail data.
`pathTrail id Z`	*id* is a pathogen id and *Z* must be one of the agent state identifiers (S, E, I, V, DI+, DD). The population array for that pathogen and for that state over time is returned.
`popTrail Z`	*Z* must be one of the agent state identifiers (S, E, I, V, DI+, DD). The array of the entire population over time for that state is returned.
`sleep T`	NMBPL processor sleeps for *T* milliseconds. (May be used for synchronization during longer simulations.)

Notes

- Commands without explicit return do not return a value
- `get` and `set` use the 3-letter "airport codes" associated with each control
- Commands may be sequenced; e.g.

  ```
  run_for 50 set XMT 1.5 run trail PATH I
  ```

  will run for 50 timesteps, set the transmission paramter to 1.5, run for another 50, and return the 100 population values of I.
- Returned values are separated by newlines. When command sequences are sent remotely, left and right brackets (i.e. \[\ and \]\) followed by newlines enclose the sequence of returned values, even if the sequence is empty; e.g.,

  ```
  [\n50\n100\n1000\n]
  ```

- When using `trail`: if embedded in a command sequence, this must be the only command that returns a value (since the array returned by each of them will be embedded in the set of answers returned by the command sequence.)
- Use the console to test command sequences before using them remotely.
- Changes to the FIFOs, if saved to Preferences, will reappear in subsequent uses. Multiple instances of Numerus can run concurrently using different FIFOs.
- **Restart** button restarts the FIFO configuration.

Figure B.3: The list of Blackbox Programming Language (BPL) commands that can be used to write a simulation driver script, using the three-letter "airport codes" listed in Table A1 to access the parameters and variables in our coded algorithm. This list of commands can be accessed using the "Command Reference" button at the bottom of the Scripting Window.

R Integration

As previously mentioned, the API supports remote control of the simulator from independent platforms using the operating system's indigenous *fifo* channels. Of particular interest is integration with the R statistical programming

medRxiv preprint doi: https://doi.org/10.1101/2021.06.07.21258504; this version posted June 11, 2021. The copyright holder for this preprint (which was not certified by peer review) is the author/funder, who has granted medRxiv a license to display the preprint in perpetuity. All rights reserved. No reuse allowed without permission.

Figure B.4: The JS scripting window accessed by selecting the "JS On" button in the main dashboard (see button second from left at bottom of Fig. 2A). The script shown here was used to execute the adaptive vaccination strategy discussed in the main text.

environment. An R-package called "seiv" acts as a driver by synchronously issuing BPL command strings and waiting for results. Consequently, a simulation can be driven entirely from within the R platform, treating the simulator as a "virtual package".

Fig. B.5 shows the code used to run the simulator multiple times with different random number generator seeds. Following each run, the time history of the population in the I, DI+ and DD states is extracted directly to an R data frame (without the need to save, for example, in a comma-separated list). At the end of the run sequence the data frame is used to build the plots shown in Fig. C.2.

R could be used in a more direct way by analyzing data at various points throughout a single run and adjusting parameters programmatically, similar to the adaptive vaccination strategy carried out in Javascript, only taking advantage of the R environment's powerful toolkit.

medRxiv preprint doi: https://doi.org/10.1101/2021.06.07.21258504; this version posted June 11, 2021. The copyright holder for this preprint (which was not certified by peer review) is the author/funder, who has granted medRxiv a license to display the preprint in perpetuity. All rights reserved. No reuse allowed without permission.

R driver used to integrate SEIV-IBM J-RAMP into runs to generate plots

```r
library("seiv")
library(ggplot2)
library(reshape)

execSEIVRemote <- function(seed=0, sampleSize=165, ...) {
  who = list(...)
  if (length(who) == 0) who = list("I", "DI+", "DD")
  seiv$dispatch(paste("reset set RSD", seed, "run_for", sampleSize))
  time <- 0:(sampleSize)
  ans <- data.frame("Time"=time)
  top <- sampleSize+1
  for (z in who) {
    nxt <- seiv$dispatch(paste("popTrail", z))
    if (length(nxt) < top) nxt = c(nxt, integer(top-length(nxt)))
    ans = cbind(ans,  nxt)
    names(ans)[length(names(ans))] = z
  }
  ans
}

multiSEIV <- function(runs=3, sampleSize=165) {
  ans = list()
  time <- 0:(sampleSize)
  for (m in 1:3) ans[[m]] = data.frame("Time" = time)
  for (n in 1:runs) {
    print(n)
    dat <- execSEIVRemote(n-1, sampleSize,  "I", "DI+", "DD")
    who <- c("I", "DI+", "DD")
    for (m in 1:3) {
      ans[[m]] = cbind(ans[[m]], dat[,c(m+1)])
      names(ans[[m]])[length(names(ans[[m]]))] = paste(who[m], "Run", n)
    }
  }
  ans
}

buildMSFrame <- function(l) {
  means = numeric()
  stds = numeric()
  for (m in 1:nrow(l)) {
    smpl = as.numeric(l[m,2:ncol(l)])
    means[m] = mean(smpl)
    stds[m] = sqrt(var(smpl))
  }
  data.frame("Time"=l[1], "μ"=means, "μ+σ"=means+stds,
             "μ-σ"=means-stds, check.names=FALSE)
}

buildGraph <- function(l, title) {
  msFrame <- buildMSFrame(l)
  molten = melt(msFrame, id.vars="Time")
  ggplot(molten, aes(x=Time, y=value, col=variable)) +
    geom_line() +
    xlab("Day") +
    ylab("Population") +
    ggtitle(title)
}

go <- function(runs=30, sampleSize=165) {
  data <- multiSEIV(runs, sampleSize)
  list (
    buildGraph(data[[1]], "Prevalence"),
    buildGraph(data[[2]], "Incidence"),
    buildGraph(data[[3]], "Daily Deaths")
  )
}
```

Figure B.5: Our SEIVD-IBM can be treated as an R-package called "seiv" and run as such in conjunction with other packages, such as ggplot2 and reshape to conduct multiple simulations and then carry out data and statistical analyses of the simulation results. The code shown here was used to produce the plots illustrated in Fig. C.2.

medRxiv preprint doi: https://doi.org/10.1101/2021.06.07.21258504; this version posted June 11, 2021. The copyright holder for this preprint (which was not certified by peer review) is the author/funder, who has granted medRxiv a license to display the preprint in perpetuity. All rights reserved. No reuse allowed without permission.

C Additional Figures

	N=10,000				N=30,000			
Run seed	**S fnl**	**V fnl**	**Total D**	**t fnl**	**S fnl**	**V fnl**	**Total D**	**t fnl**
0	2135	7700	165	166	6574	22964	462	212
1	2234	7522	144	171	6431	23067	502	193
2	2252	7602	146	158	6516	23020	464	175
3	2174	7668	158	188	6568	22958	474	220
4	2154	7684	162	162	6345	23214	441	191
5	2127	7706	167	165	6520	22998	482	196
6	2166	7662	172	159	6604	22950	446	198
7	2280	7573	147	171	6282	23250	468	197
8	2254	7613	133	161	6339	23184	477	187
9	2153	7681	166	169	6529	23050	421	201
Mean	**2193**	**7641**	**156**	**167**	**6471**	**23066**	**464**	**197**
SD	**56**	**61**	**13**	**9**	**114**	**112**	**23**	**13**
Mean %	0.219	0.764	0.0156		0.216	0.769	0.0155	
SD %	0.006	0.006	0.0013		0.004	0.004	0.0008	

Figure C.1: The final sizes of the uninfected ($S(t_{\text{fnl}})$ individuals), infected ($V(t_{\text{fnl}})$ individuals) and dead ($D(t_{\text{fnl}})$ individuals) classes and the length of the epidemic (t_{fnl} days) are provided here, together with summary statistics, for 10 simulations (runtime seed ranges from 0 to 9) in each case when the initial population sizes are $N_0 = 10,000$ and $N_0 = 30000$ individuals respectively. The parameter values used are otherwise the same as those use to produce the simulation depicted in Fig. 2 in the main text.

medRxiv preprint doi: https://doi.org/10.1101/2021.06.07.21258504; this version posted June 11, 2021. The copyright holder for this preprint (which was not certified by peer review) is the author/funder, who has granted medRxiv a license to display the preprint in perpetuity. All rights reserved. No reuse allowed without permission.

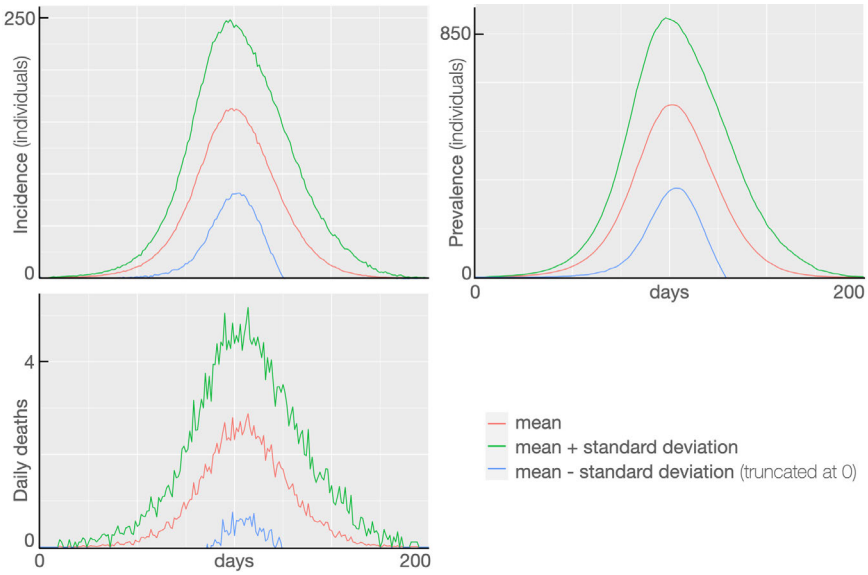

Figure C.2: Plots of the mean (red) ± 1 standard deviation green and blue, the latter truncated at 0) of prevalence, incidence, and daily deaths for 100 runs (runtime seeds = 0,...,99) using the same parameter set used to produce the individual run (runtime seed = 0) depicted in Fig. 2 in the main text (also see Fig. C.1). These figures where produced by running our SEIVD-IBM J-RAMP as an R-package as described in Appendix B, with the code documented in Fig. B.5.

medRxiv preprint doi: https://doi.org/10.1101/2021.06.07.21258504; this version posted June 11, 2021. The copyright holder for this preprint (which was not certified by peer review) is the author/funder, who has granted medRxiv a license to display the preprint in perpetuity. All rights reserved. No reuse allowed without permission.

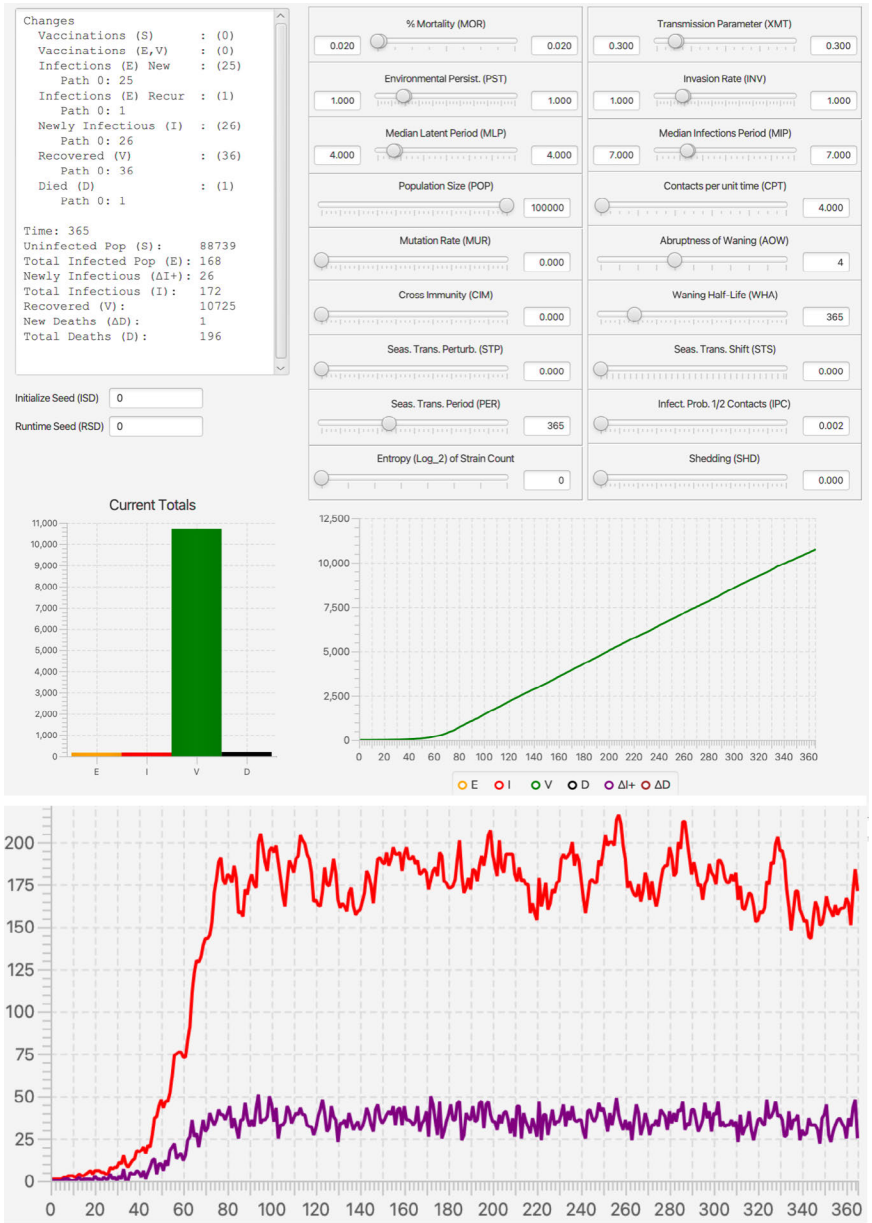

Figure C.3: If, together with our basic set of parameters (Table 1), we set $p_{\mathrm{I}}^{\mathrm{half}} = 0.005$ then the total number of individuals that have been infected (disease class V) at the end of one year is $10027/100,000 \approx 10\%$.

medRxiv preprint doi: https://doi.org/10.1101/2021.06.07.21258504; this version posted June 11, 2021. The copyright holder for this preprint (which was not certified by peer review) is the author/funder, who has granted medRxiv a license to display the preprint in perpetuity. All rights reserved. No reuse allowed without permission.

Strain	beta	Strain	beta	Strain	beta	Strain	beta	Strain	beta	Strain	beta	Strain	beta	Strain	beta
0	0.300	16	0.149	32	0.246	48	0.295	64	0.235	80	0.152	96	0.196	112	0.272
1	0.325	17	0.097	33	0.244	49	0.076	65	0.121	81	0.127	97	0.172	113	0.233
2	0.007	18	0.117	34	0.011	50	0.289	66	0.249	82	0.138	98	0.177	114	0.261
3	0.350	19	0.089	35	0.029	51	0.155	67	0.079	83	0.019	99	0.165	115	0.122
4	0.252	20	0.222	36	0.162	52	0.043	68	0.133	84	0.258	100	0.037	116	0.089
5	0.217	21	0.292	37	0.214	53	0.110	69	0.127	85	0.181	101	0.087	117	0.063
6	0.105	22	0.222	38	0.102	54	0.263	70	0.136	86	0.042	102	0.230	118	0.299
7	0.375	23	0.214	39	0.036	55	0.049	71	0.184	87	0.284	103	0.096	119	0.230
8	0.214	24	0.205	40	0.010	56	0.037	72	0.166	88	0.218	104	0.219	120	0.122
9	0.256	25	0.100	41	0.173	57	0.108	73	0.015	89	0.249	105	0.058	121	0.200
10	0.217	26	0.089	42	0.093	58	0.201	74	0.048	90	0.025	106	0.033	122	0.131
11	0.151	27	0.026	43	0.256	59	0.041	75	0.131	91	0.052	107	0.219	123	0.207
12	0.009	28	0.296	44	0.236	60	0.159	76	0.013	92	0.160	108	0.151	124	0.272
13	0.077	29	0.065	45	0.038	61	0.053	77	0.207	93	0.121	109	0.005	125	0.001
14	0.026	30	0.019	46	0.186	62	0.186	78	0.019	94	0.234	110	0.110	126	0.115
15	0.400	31	0.425	47	0.078	63	0.450	79	0.149	95	0.165	111	0.214	127	0.475

Figure C.4: This is the set of strain transmission parameter values $\beta_j, j = 0, ..., 127$ used in our 128 strain simulation. Note strains 0, 1, 3, 7, 15, 63, 127 (light blue cells) are part of a dominating sequence of values increasing steadily in steps of 0.025 from $\beta_0 = 0.30$ to $\beta_{127} = 0.475$ along the one-step-neighborhood pathway represented by the allele structures (0,0,0,0,0,0,0), (0,0,0,0,0,0,1), (0,0,0,0,0,1,1),...,(1,1,1,1,1,1,1). All the remaining β values were generated at random on the interval $[0, 0.3]$.

medRxiv preprint doi: https://doi.org/10.1101/2021.06.07.21258504; this version posted June 11, 2021. The copyright holder for this preprint (which was not certified by peer review) is the author/funder, who has granted medRxiv a license to display the preprint in perpetuity. All rights reserved. No reuse allowed without permission.

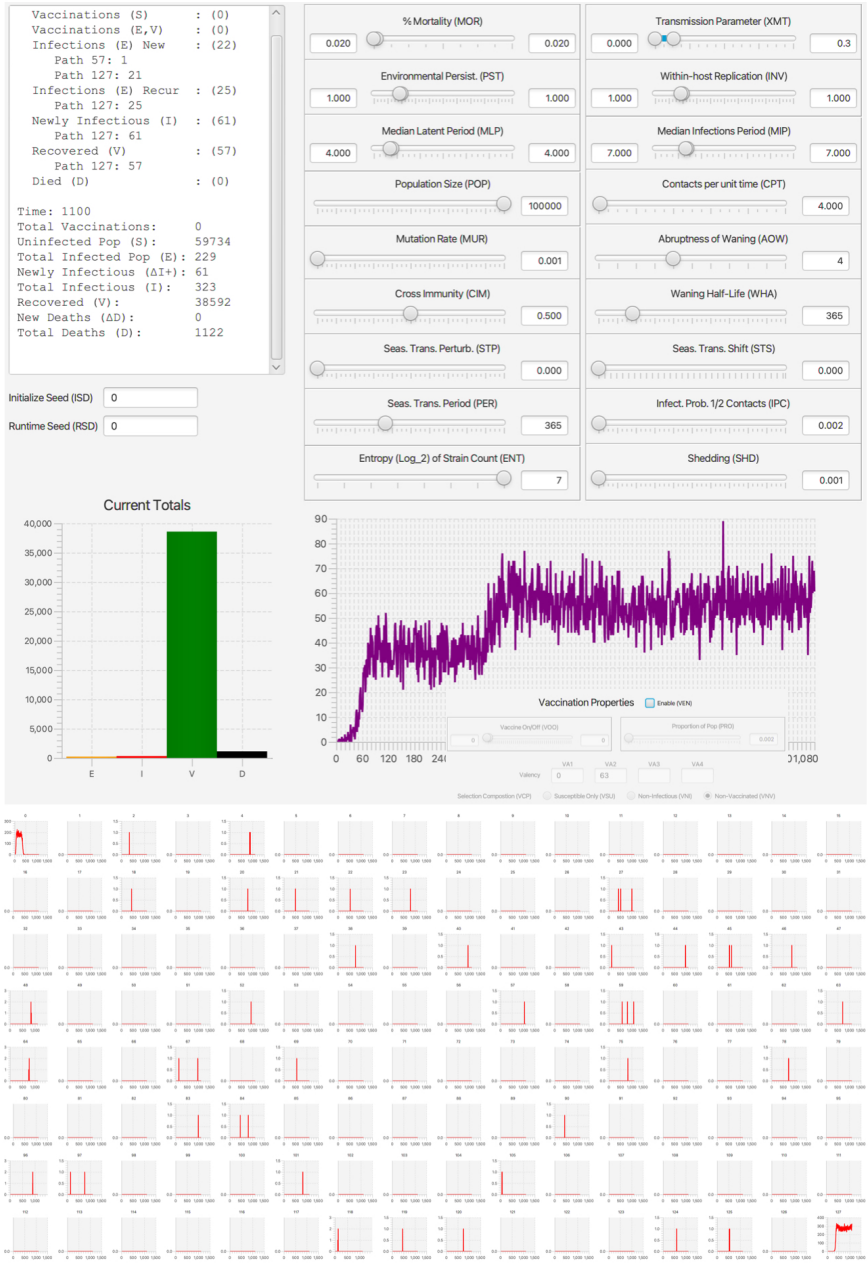

Figure C.5: This is a baseline 3-year no vaccination run for our 128-strain vaccination study with strain-specific transmission values depicted in Fig. C.4 and other parameter values as indicated on the dashboard (also see Table 1). See Fig. 6 in main text for enlarged plots of predominant strains.

medRxiv preprint doi: https://doi.org/10.1101/2021.06.07.21258504; this version posted June 11, 2021. The copyright holder for this preprint (which was not certified by peer review) is the author/funder, who has granted medRxiv a license to display the preprint in perpetuity. All rights reserved. No reuse allowed without permission.

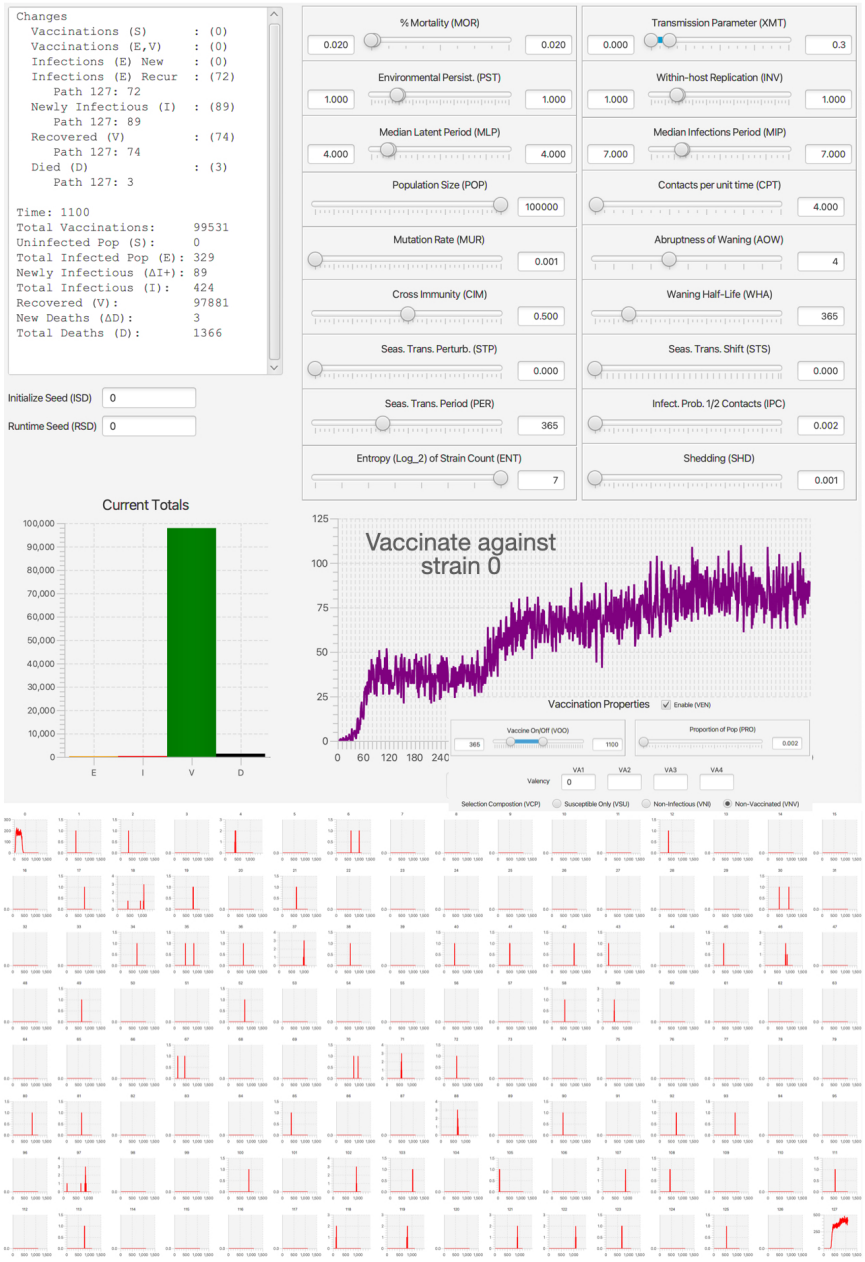

Figure C.6: This is vaccination in years 2 and 3 against strain 0 at the rate of 0.2% of the population per day in our 128-strain vaccination study with strain-specific transmission values depicted in Fig. C.4 and other parameter values as indicated on the dashboard (also see Table 1). See Fig. 6 in main text for enlarged plots of predominant strains.

medRxiv preprint doi: https://doi.org/10.1101/2021.06.07.21258504; this version posted June 11, 2021. The copyright holder for this preprint (which was not certified by peer review) is the author/funder, who has granted medRxiv a license to display the preprint in perpetuity. All rights reserved. No reuse allowed without permission.

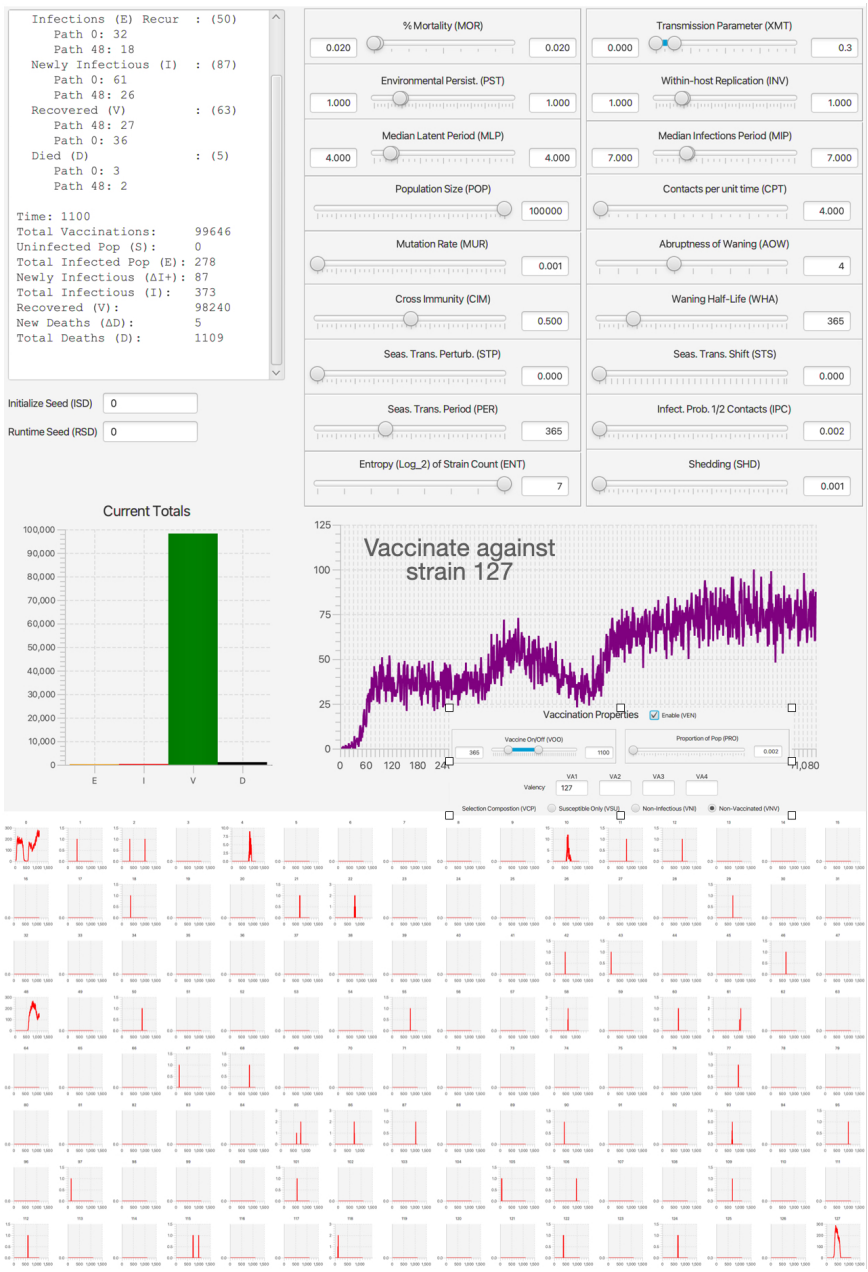

Figure C.7: This is vaccination in years 2 and 3 against strain 127 at the rate of 0.2% of the population per day in our 128-strain vaccination study with strain-specific transmission values depicted in Fig. C.4 and other parameter values as indicated on the dashboard (also see Table 1). See Fig. 6 in main text for enlarged plots of predominant strains.

medRxiv preprint doi: https://doi.org/10.1101/2021.06.07.21258504; this version posted June 11, 2021. The copyright holder for this preprint (which was not certified by peer review) is the author/funder, who has granted medRxiv a license to display the preprint in perpetuity. All rights reserved. No reuse allowed without permission.

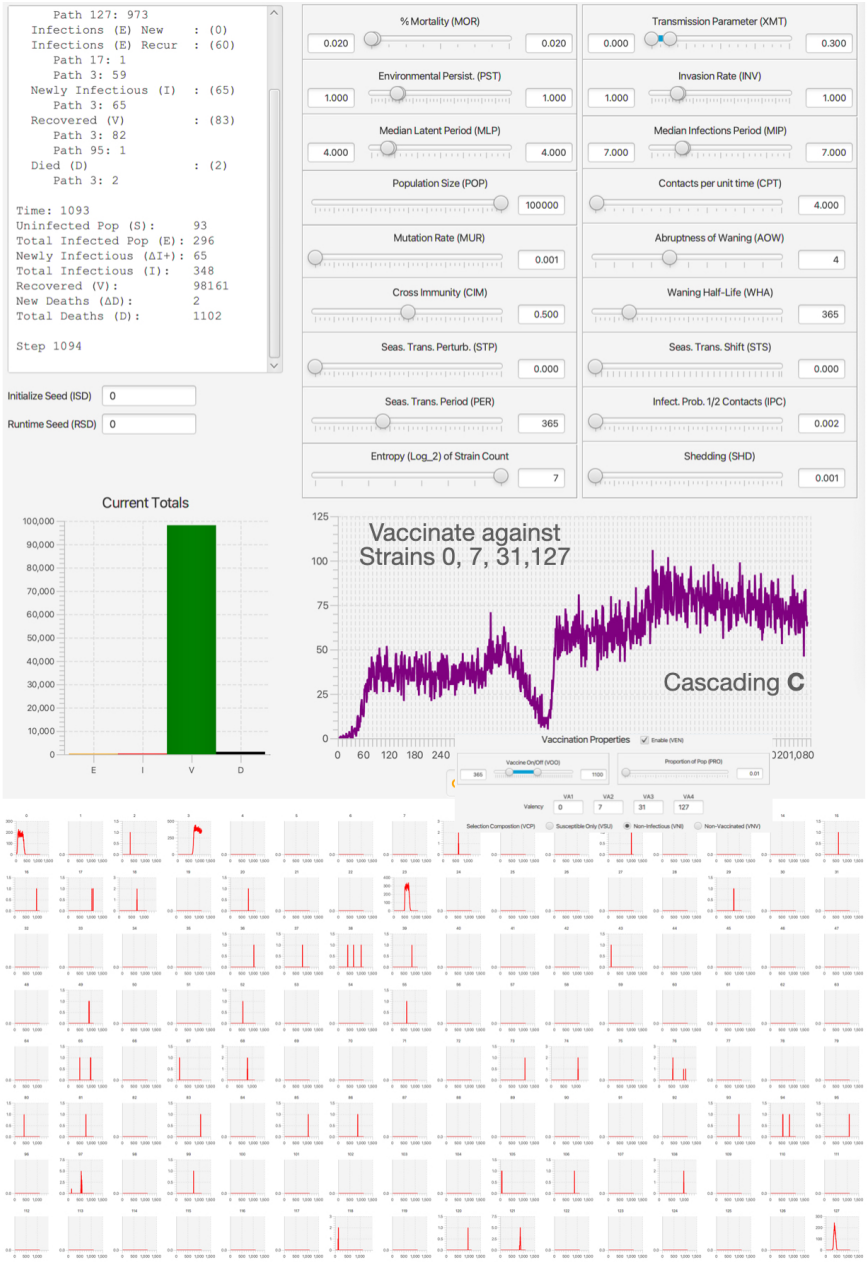

Figure C.8: This is a multivalent vaccination in years 2 and 3 against strains 0, 7, 31 and 127 at the rate of 1.0% of the population per day in our 128-strain vaccination study with strain-specific transmission values depicted in Fig. C.4 and other parameter values as indicated on the dashboard (also see Table 1), except that the cross immunity matrix **C** is now defined by Eq. A.7. See Fig. 6 in main text for enlarged plots of predominant strains.

medRxiv preprint doi: https://doi.org/10.1101/2021.06.07.21258504; this version posted June 11, 2021. The copyright holder for this preprint (which was not certified by peer review) is the author/funder, who has granted medRxiv a license to display the preprint in perpetuity. All rights reserved. No reuse allowed without permission.

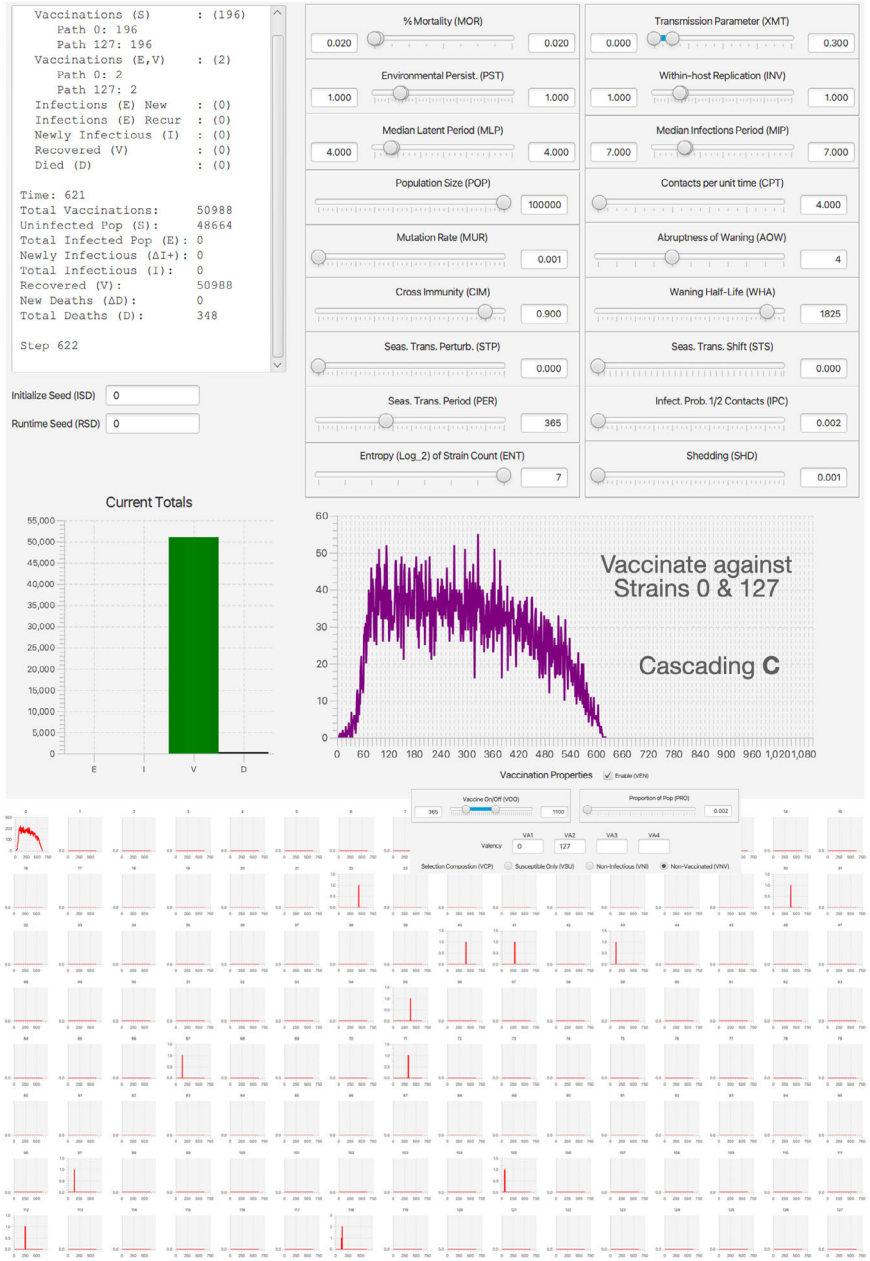

Figure C.9: This is a bivalent vaccination in years 2 and 3 against strains 0 and 127 at the rate of 0.2% of the population per day in our 128-strain vaccination study with strain-specific transmission values depicted in Fig. C.4 and other parameter values as indicated on the dashboard (also see Table 1), except that the half-wining values has been increased fivefold $t^{\text{half}} = 1825$ days the cross immunity matrix $\mathbf{C}$ is now defined by Eq. A.7 with $c = 0.9$. See Fig. 6 in main text for enlarged plots of the predominant strain 0.